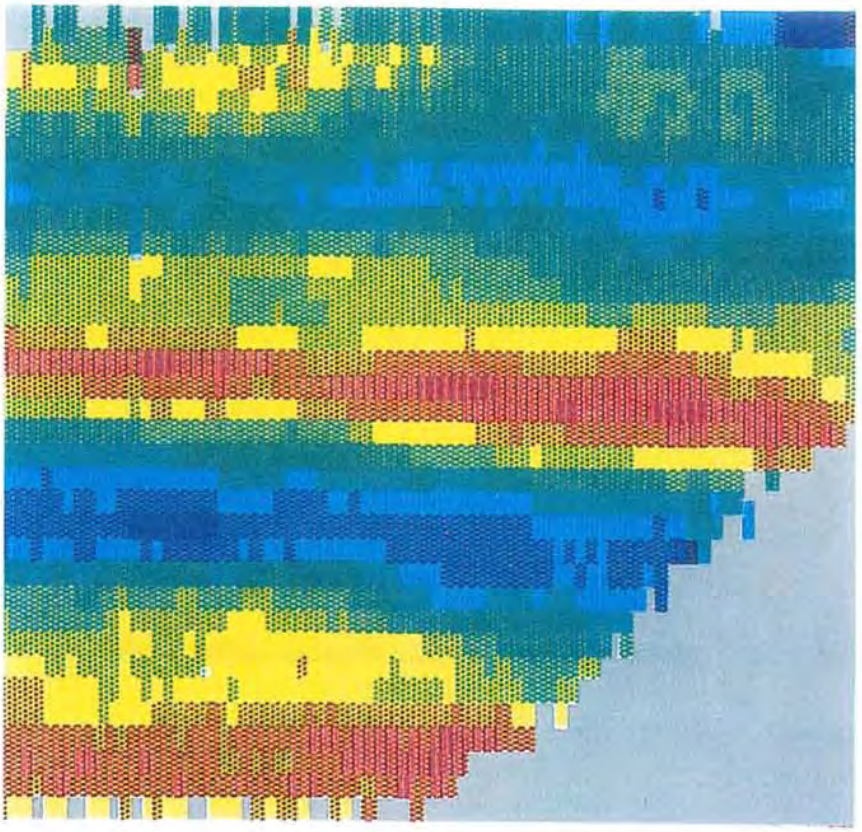

EISCAT

EUROPEAN INCOHERENT SCATTER SCIENTIFIC ASSOCIATION

ANNUAL REPORT 1989

S-981 28 KIRUNA, SWEDEN

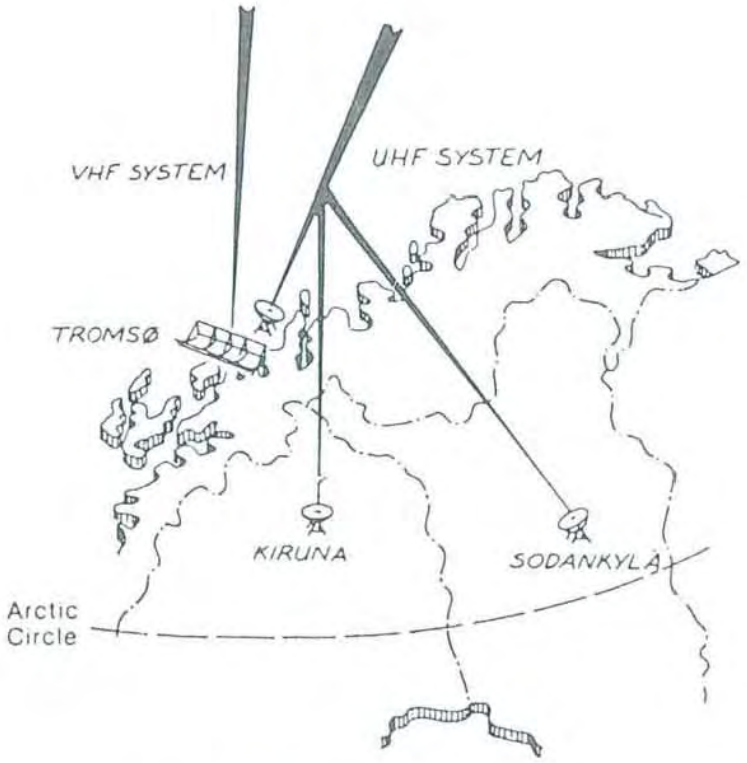

The EISCAT Radar Systems

(see page 2 for a more detailed description)

The cover illustration is a colour representation of the meridional wind velocities in the altitude range 55 to 80 km measured by the EISCAT UHF radar operating the Unusual Programme, UP-1. The data depicted span the time interval 1300 to 1530 UT on 23 October 1989. These measurements were made possible by the precipitation of energetic protons deep into the atmosphere during a solar proton event (SPE) where they caused both D-region ionization and the resulting polar cap absorption (PCA) of radio signals. Such events occur preferentially near sunspot maximum, as was the case in 1989 when several similar data sets were obtained. The enhanced echoes from the D-region during SPE's support important studies of neutral atmosphere dynamics in this region, which is normally inaccessible by radar. The colour scale runs from red, representing winds blowing southward at 50 m s^{-1}, through green, corresponding to zero motion, to blue, which represents northward winds of 50 m s^{-1}.

ANNUAL REPORT 1989

EISCAT, *the European Incoherent Scatter Scientific Association, is established to conduct research on the middle and upper atmosphere, ionosphere and aurora using the incoherent scatter radar technique. This technique is the most powerful ground-based tool for these research applications. EISCAT is also being used as a coherent scatter radar for studying instabilities in the ionosphere as well as for investigating the structure and dynamics of the middle atmosphere and as a diagnostic instrument in ionospheric modification experiments (Heating).*

There are seven incoherent scatter radars in the world, and EISCAT operates two of the highest-standard facilities. The experimental sites of EISCAT are located in Scandinavia, north of the arctic circle. They consist of two independent radar systems (see schematic on the inside of the front cover).

The EISCAT UHF radar operates in the 931 MHz band with a peak transmitter power of 1.5 MW and 32 m, fully steerable parabolic dish antennas. The transmitter and one receiver are in Tromsø (Norway). Receiving sites are also located near Kiruna (Sweden) and Sodankylä (Finland), allowing continuous tristatic measurements to be made.

The monostatic VHF radar in Tromsø operates in the 224 MHz band with a peak transmitter power of 1.5 MW (to be raised to 4 MW) and a 120 m x 46 m parabolic cylinder antenna, which is subdivided into four sectors. It can be steered mechanically in the meridional plane from 30° south to 60° north of the zenith.

The basic data measured with the incoherent scatter radar technique are profiles of electron density, electron and ion temperature and ion velocity. Subsequent processing also allows a wealth of further parameters, describing the ionosphere, upper atmosphere and mesosphere, to be derived from these. A selection of well-designed radar pulse schemes allows the adaptation of the data-taking routines to many particular phenomena, occurring at altitudes between about 60 km and more than 1000 km. Depending on geophysical conditions, a best time resolution of better than one second and an altitude resolution of a few hundred meters can be achieved, whereas typical resolutions are of the order of minutes and kilometres.

Each year, 2000 operating hours (nominal) are distributed equally between Common Programmes (CP) and Special Programmes (SP). At present six well-defined Common Programmes are run regularly for 24 hours, or more, about 30 times per year to provide a data base for long term synoptic studies. Three Unusual Programmes (UP) are started ad hoc during particular geophysical conditions. A large number of Special Programmes, defined individually by associate scientists, are run to study a variety of specific geophysical events.

The Annual Reports present a summary of EISCAT's operations, developments, scientific results, publications and budget for each year. Further details of the EISCAT system and operation can be found in various EISCAT reports, including an illustrated brochure, which can be obtained from EISCAT Headquarters in Kiruna, Sweden.

The investments and operational costs of EISCAT are shared between:

Suomen Akatemia, Finland
Centre National de la Recherche Scientifique, France
Max-Planck-Gesellschaft, Federal Republic of Germany
Norges Almenvitenskapelige Forskningsråd, Norway
Naturvetenskapliga Forskningsrådet, Sweden
Science and Engineering Research Council, United Kingdom

EISCAT ANNUAL REPORT 1989
CONTENTS

	page
Council Chairman's Forward	4
Director's Introduction	5
Operations	
The Year in Pictures	11
Catalogue of Observations	12
Scientific Research and Developments	
Mesosphere and D-region	13
E-Region Studies	16
F-Region Studies	21
Auroral Investigations	21
High-latitude Convection/Magnetospheric Responses	29
Non-thermal Plasmas	28
Other Scattering Phenomena	37
Ionospheric Modification (Heating)	39
Digital Signal Processing	41
Appendices	
Publications	
1989 Journals	43
Other Publications	46
EISCAT Reports and Meetings	48
Budget Balance Sheet 1989	49
EISCAT Council, Committees and Senior Staff	50
The EISCAT Associates	51
Addresses	Back Cover

Annual Report 1989 of the EISCAT Scientific Association

Editing and lay-out by:
Tony van Eyken and Jürgen Röttger,
EISCAT Headquarters, Kiruna, Sweden

Finishing and Printing by:
Birgitta Määttä and Stig Björklund,
Institutet för Rymdfysik, Kiruna, Sweden

ISSN 0349-2710

COUNCIL CHAIRMAN'S PAGE

This year has been a very successful one for EISCAT. Many outstanding problems have been resolved, new initiatives started and, above all, excellent science has been produced. Demand for EISCAT time remains high and once again the system has been operated for slightly longer than the nominal 2000 hours in order to satisfy user requests. New Common Programmes have been introduced and it is particularly gratifying to note that the VHF Common Programmes are now operational.

Major progress has been made with the elimination of the problems of interference caused by the Nordic radio telephone system. However, some difficulties still remain with regard to VHF interference at Tromsø. All those involved are to be congratulated for their efforts to reach mutually acceptable solutions to these difficulties. Some VHF klystron problems are still with us, although satisfactory operation of the VHF transmitter has been possible during the year.

A major extension of EISCAT activities will result from the take-over of the Max-Planck-Institut für Aeronomie Heating facility at Tromsø. This will add a new dimension to the kind of science that EISCAT can undertake and we are greatly indebted to the Max-Planck-Gesellschaft and the research councils of the Associate countries for providing the financial support for this important development. Following an invitation from one of the Associate countries, EISCAT is planning to become involved in a new Polar Cap Incoherent Scatter Radar (PCR) to be located on Spitzbergen. It is envisaged that this new radar will form an extension of the EISCAT facilities to the polar cap regions. Collaboration in this project is being actively encouraged with a view to forming a group to produce a system design for the PCR.

There have been a number of staff changes during the year. I would like to thank those who have left, for their contributions to EISCAT, and welcome those who have joined during the year. My particular thanks go to the Director and his staff for their help and guidance during my first year as Chairman.

Tudor Jones

DIRECTOR'S INTRODUCTION

The year 1989 was one of good progress though a few misfortunes appeared and continue to hamper the full VHF operation. On the average, however, the UHF system is in a very healthy shape and the VHF system undergoes a systematic upward trend, which is demonstrated for instance by the new science resulting from many VHF experiments. I am pleased to report about the major events, highlights and developments of EISCAT in this introduction to the Annual Report 1989.

Several Special Programme campaigns took place and the Common Programme operation continued as usual. Previously, Common Programmes used only the UHF system, but now VHF Common Programmes have also been successfully tested, for example the D-region/mesosphere programme CP-6 and the high-altitude programme CP-7. Overall, VHF Common Programme operations amounted to 79 hours, equivalent to 7% of the total Common Programme time of 1115 hours. Also the new UHF Common Programmes CP-4, (high-latitude programme) and CP-5 (optimised for lower thermosphere studies), were run for extended periods of about 100 hours each to serve the purposes of World Day campaigns for GISMOS (Global Ionospheric Simultaneous Measurements of Substorms) and LTCS (Lower Thermosphere Coupling Study). Close to 100% of the Common Programme data have been analyzed, which is a good sign of the high reliability of the system. It is now also possible to routinely obtain the full vector velocities during Common Programmes by combining the data from all sites in real-time. Several Unusual Programmes operations took place, mostly to take data with the low-altitude UHF programme UP-1 during some of the strong solar proton events which occurred during 1989. The front cover of this Annual Report shows the meridional velocities in the mesosphere revealed by enhanced electron density during such a solar proton event. At times the UHF radar and the VHF radar were also operated simultaneously.

Special Programmes were conducted over 1157 hours. Together with the Common Programme operation this adds up to a total of 2272 hours of EISCAT experiment operation during the year 1989. This is again higher than the target of 2000 hours and indicates both the strong demand for experiment time by Associate scientists and participation in longer World Day operations as well as the high reliability of the system. The percentage of Special Programme operations per Associate in the year 1989 (the values in brackets give the accumulated usage) were:

France	37%	(25%)
United Kingdom	25%	(28%)
Germany	17%	(21%)
Sweden	8%	(9%)
Norway	7%	(9%)
EISCAT	5%	(5%)
Finland	1%	(3%)

More than 150 hours (13%) of the Special Programme operation were with the VHF system, although this is still limited to 1.5 MW peak power, and beam directions between north and vertical only. A breakdown of operations in 1989 can be found on pages 11 and 12.

The total number of data tapes handled by EISCAT in the year 1989 amounts to almost 1700, of which 90 were analysed Common Programme data. These are regularly distributed to the data representatives of the Associates and those for the World Day operations are also sent to the Incoherent Scatter Radar Data Base at NCAR in Boulder.

The Headquarters computer was upgraded by providing access to a new Norsk Data ND 5400, which is shared between EISCAT and the Swedish Institute of Space Physics (IRF) in Kiruna. The general evolution of the computing systems at the EISCAT sites and Headquarters is directed towards a gradual change to local area networks of workstations and industrial-standard PCs. It is anticipated that these arrangements will allow flexible and reliable operations, enriched data analyses by EISCAT staff and visitors and will make EISCAT more independent of single computer suppliers. In the context of data acquisition evolution, the integrator-decoder project

(MUFFIN) to allow on-line decoding of the newly applied alternating and complementary codes, has made further progress at the Sodankylä site. Another project, shared with the IRF, is the design of a new digital spectrum analyzer (FFT Processor), which will allow high speed on-line spectrum analysis. The memories of the present radar controllers are being extended from 4 kWords to 32 kWords, which allows the application of more sophisticated codes. It is now also possible to preload codes into the buffer memory, which permits some alternating pulse schemes to be decoded on-line using an additional hardware decoder installed in the correlator as described on page 41 of this report.

Substantial improvements have been achieved in eliminating the effects of the NMT 900 mobile telephone transmitters on our receiving systems in Kiruna and Sodankylä. This became possible through the insertion of special bandpass filters and high power mixers; the local oscillators have also been exchanged and modified to reduce noise sidebands. It is, for instance, again possible to perform observations with such extreme requirements as those of radio astronomy. The Tromsø receiver front end has also been improved to optimize the transmit-receive transition effects and further reduce the noise figure. The UHF transmitter continues to be one of the most reliable parts of the system and it is operated continuously for many days during extended World Day and Special Programme campaigns at power levels of 1.5 MW and full duty cycle.

In the course of routine system maintenance, inspections of the VHF and UHF antennas were made by outside experts in spring 1989. The antennas were found to be in generally good shape and, in addition, we are now proceeding with further improved preventive maintenance and inspection procedures. Particularly the summer months are being used for this purpose, such as work on pintle bearings, oil exchange, sealing of bearings, rail and basement inspections and repair and painting of steel members and surface elements of the VHF antenna. Special arrangements have been worked out for safe-guarding the antenna in Sodankylä when the water level of the nearby Kitinen river will be raised in a few years.

The VHF transmitter was still operated with only one klystron at 1.5 MW and reduced duty cycle of 7.5%. In the beginning of the year 1989 we experienced a break of the filament of klystron YK1320/2, and this klystron was returned for repair to the factory in Hamburg. After inspection it was decided to redesign the filament construction and to exchange the heater transformers. Because of leaks in the klystron output coupling, which occurred during the factory processing, the replacement of certain material parts were also considered. This has delayed the replacement of this klystron YK1320/2 into the year 1990.

The rebuilt klystron YK1320/1, which had been installed in Tromsø in autumn 1988, was used successfully in experiments. It was not possible to accept this klystron at that time, but EISCAT was permitted to run it with reduced operating parameters. A break of a cooling pipe and flooding of part of the transmitter happened in July. This did not affect the performance of the klystron but destroyed some of the magnet coils. Further adjustments and tests of the klystron followed, during which a vacuum leak occurred, which was fixed by the Philips engineers on site in Tromsø. The acceptance test performed in October 1989 showed output power of the order of 2 MW, which is less than the specifications. The resulting negotiations on payment reductions continue into the year 1990.

Because of all the uncertainties experienced, we decided to prepare a feasibility study for an alternative VHF transmitter, which could be used in case both klystrons eventually fail. Such a VHF transmitter could use gridded tubes, instead of klystrons, and would further allow an electronic east-west antenna beam steering.

The interference, which is still caused in the immediate neighbourhood by the VHF operation, results from spill-over from the antenna reflector surface when the antenna beam is pointing south of the zenith. We have investigated several possibilities to mitigate these spill-over effects, such as fencing the antenna, extending the reflector surface or changing the feed system mechanically or electrically, in addition to electronic hardening and shielding of affected equipment. Only the latter measures appear to be feasible and we have made good progress in this work. It can now be noted that the VHF system interference and radiation situation has

improved and EISCAT in its present configuration, with vertical and northward beam directions, is certainly operating well below official hazard limits. Since new equipment may be brought into the neighbourhood, and could be affected by the EISCAT operation, we have to continue the elaborate work on interference mitigation by improving the shielding and screening of equipment and houses in order to eliminate any further complaints. This work is particularly important for the planned VHF antenna configuration which should allow the automatic electronic west-east steerability of the antenna beam.

Following long procedures and negotiations with the telecommunication administrations of Norway, Sweden and Finland, the prolongation of the operating permit for the EISCAT Tromsø transmitters was issued at the end of the year 1989. In principal, this permission is valid until 1998, but it needs to be reconsidered every two years in order to take into account changing operating conditions and frequency allocations to other radio systems in or close to the EISCAT bands. The issue of the operating permit is recognised with great appreciation to the telecommunication administrations and it is expected that the operating conditions imposed on EISCAT are acceptable.

Many visiting scientists spent time in Kiruna, Tromsø and Sodankylä to perform experiments with the EISCAT radars and also brought their own instrumentation, such as optical devices and digital instruments. The visitors and operators can now use a redesigned control room in Tromsø which separates the control and monitor terminal devices from the radar control, monitor and acquisition instruments. Many visitors from the general public enjoyed tours of the EISCAT sites and EISCAT participated also at the Technical Exhibition in Stockholm in autumn 1989. For this purpose a special leaflet, describing the EISCAT Scientific Association, its structure and operation, the scientific goals and the scientific results, was prepared. This leaflet is reproduced in Table 1. We have also prepared a special computer slide show for a tutorial introduction to the incoherent scatter technique using EISCAT. The French Associate has made available a copy of the video movie 'Nuit d'Aurores: les relations soleil-terre', of which an English translation was prepared for distribution to all Associates. In August we appreciated the visit of the Chairman of the Astronomy and Planetary Science Board of the Science and Engineering Research Council of the United Kingdom, Professor Arnold Wolfendale, and the Secretary of the EISCAT Council Chairman, Ian Midson, to the Tromsø site. The Director and other staff members showed him the site and its operation, see Fig. 1. In November the EISCAT Council Chairman, Professor Tudor B. Jones, paid a visit to the Tromsø site.

Fig. 1. In August 1989 Professor Arnold Wolfendale, Chairman of the SERC Astronomy and Planetary Science Board, together with the Secretary of the EISCAT Council Chairman, Ian Midson, visited the EISCAT Tromsø site. The photo shows (from front to back) Professor A. Wolfendale, Dr. J. Röttger, Dr. A.P. van Eyken and Mr. I. Midson next to the end of the VHF antenna feeder bridge.

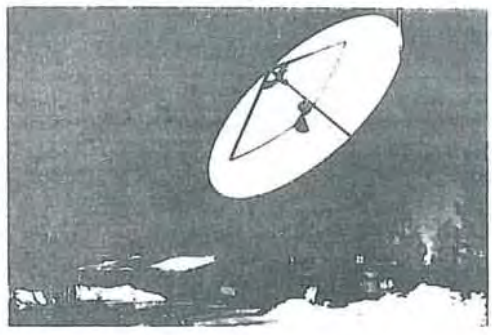

EUROPEAN INCOHERENT SCATTER SCIENTIFIC ASSOCIATION

S-981 28 KIRUNA, SWEDEN

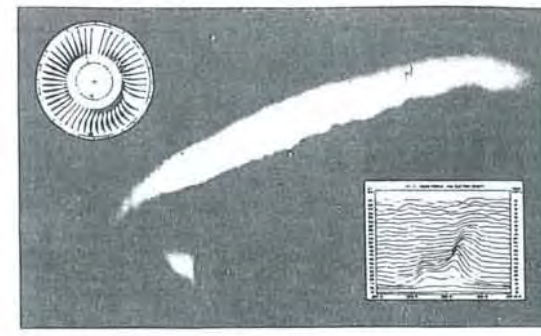

EISCAT, the European Incoherent Scatter Scientific Association, is established to conduct research on the middle and upper atmosphere, ionosphere and aurora using the incoherent scatter radar technique. This technique is the most powerful groundbased tool for these research applications. EISCAT is also being used as a coherent scatter radar for studying plasma instabilities in the ionosphere as well as for investigating the structure and dynamics of the middle atmosphere and as a diagnostic instrument in ionospheric plasma modification experiments (Heating).

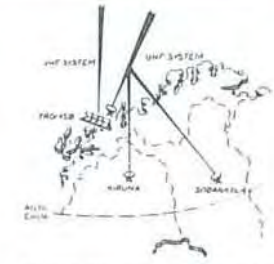

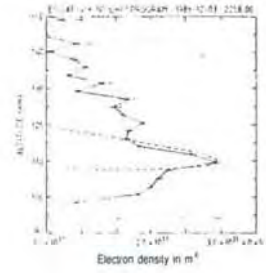

The basic data, which are measured with the incoherent scatter radar technique, are the profiles of electron density (left hand diagram), electron and ion temperature and ion velocity. A selection of well-designed radar pulse schemes allows the adaption of the data taking routines to many particular phenomena, occurring at altitudes between about 60 km and more than 1000 km. Depending on geophysical conditions, a best time resolution of one second and an altitude resolution of a few hundred meters can be achieved, whereas typical resolutions are in the order of minutes and kilometers.

SOME RESULTS OF EISCAT RESEARCH

Auroral Arcs and the Ionospheric E- and D-Region

On the right is an example of EISCAT observations of a particular class of auroral forms called Omega bands. The diagram shows the reconstructed two-dimensional distribution of conductivity and electric field deduced from EISCAT incoherent scatter radar together with magnetometer data. This ionospheric signature closely matches the observed auroral structure. These observations are necessary to promote the insight into auroral electrodynamics.

The diagram above shows contours of ionospheric absorption, caused by enhanced ionization in the D-region, as measured by EISCAT, compared with the total radio frequency absorption as measured by a riometer (a device which measures the absolute intensity of cosmic radiation in a certain frequency band). Energy spectra of precipitating auroral particles, which cause this ionization, can be retrieved and the effect of absorption on radio communications can be better understood.

The lower plot shows a recently discovered phenomenon which causes very strong, frequently wavelike, echoes to be generated by ionospheric irregularities which lie at altitudes of about 85 km in the summertime atmosphere. The existence of these echoes at the EISCAT VHF, and sometimes even UHF, frequencies poses exciting challenges for the theory of irregularity formation in the neutral and the ionized atmosphere, and will foster understanding of its chemistry and physics.

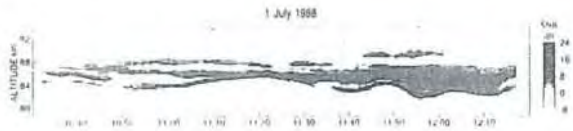

Magnetosphere, Thermosphere and Ionospheric F-region

In the upper left-hand corner of the aurora display on the backside of this page is a polar projection showing the large scale distribution of field aligned currents between the ionosphere and magnetosphere, deduced from EISCAT Common Programme data in the latitudes 65°-75°N over the period of 24 hours. The clear reversals in current flow associated with the polar cap boundary have been used to combine this data with point measurements made by satellite-borne instruments. This proves that the combination of ground-based and space-borne observations is extremely useful for explaining the effects of magnetosphere-ionosphere coupling.

This panel shows thermospheric winds in the neutral atmosphere which have been derived from EISCAT data and the corresponding wind velocities deduced from optical, Fabry-Perot interferometer measurements. The latter are limited to periods of local clear skies and hours of darkness, whereas the EISCAT observations do not suffer from such limitations. Knowledge of thermospheric winds is needed to refine the global circulation models.

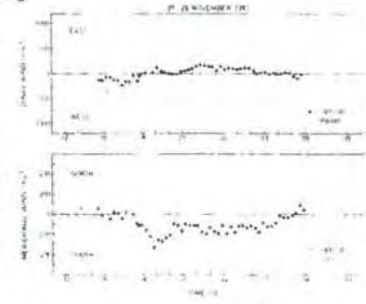

The inset diagram in the lower right-hand corner of the aurora display on the backside shows very high time resolution density data from altitudes between 100 km and 300 km. The leading edge of an electron density enhancement associated with a visible auroral fold enters the radar view at low altitudes and is seen progressively later at greater altitudes, as the structure moves across the static radar beam. Such observations improve substantially the understanding of the complex processes leading to the aurora.

Ionospheric Modification

This panel shows a power-frequency spectrum of the radar return from a region in the ionosphere around 200 km, which has been artificially heated by a strong HF radio wave transmitted from the ground. The heating and electrostatic forcing drive the plasma into a non-linear regime where instabilities are formed. These scatter the radar signal, which thus becomes a diagnostic tool for studying plasma physical processes in the ionosphere.

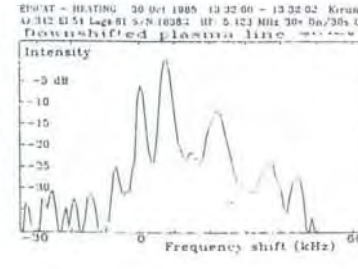

Table 1: The EISCAT Leaflet

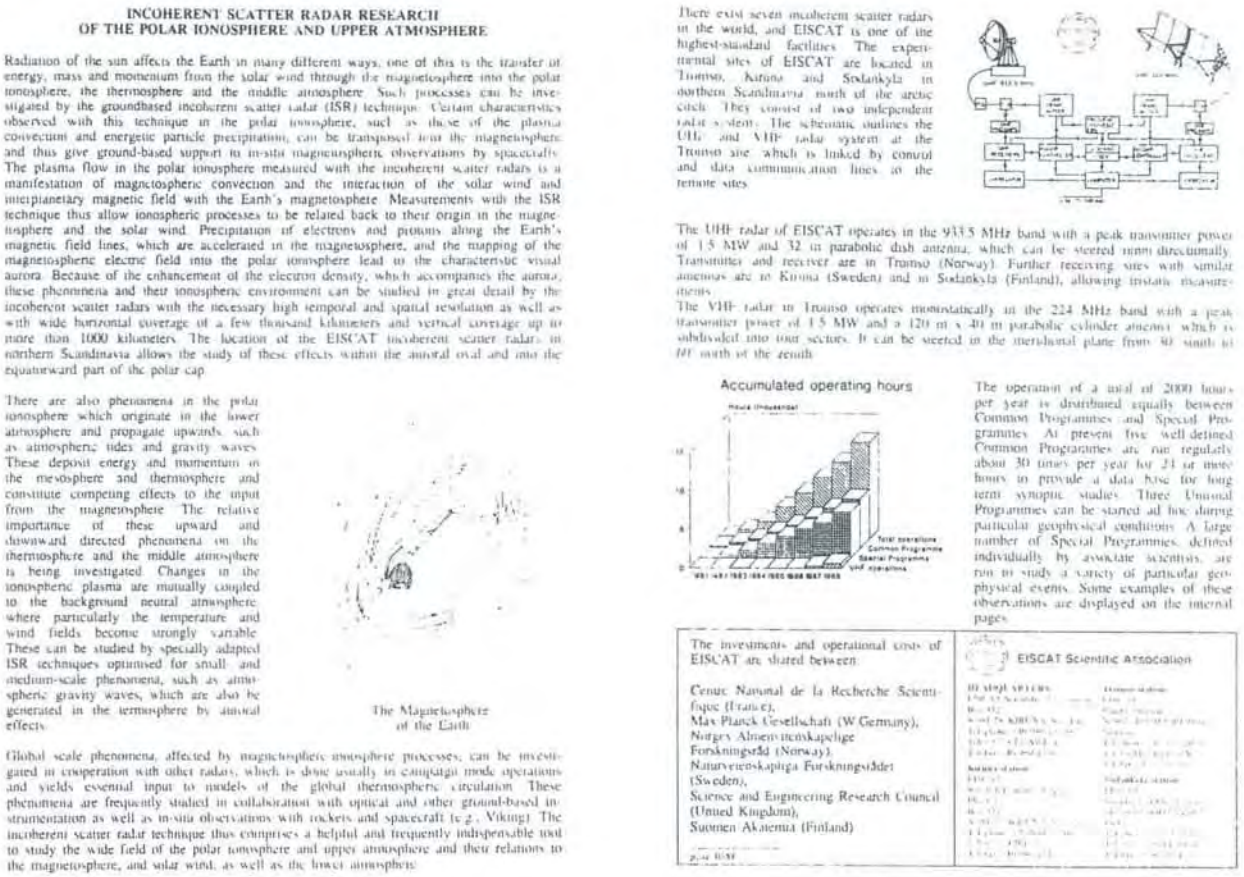

INCOHERENT SCATTER RADAR RESEARCH
OF THE POLAR IONOSPHERE AND UPPER ATMOSPHERE

Radiation of the sun affects the Earth in many different ways, one of this is the transfer of energy, mass and momentum from the solar wind through the magnetosphere into the polar ionosphere, the thermosphere and the middle atmosphere. Such processes can be investigated by the groundbased incoherent scatter radar (ISR) technique. Certain characteristics observed with this technique in the polar ionosphere, such as those of the plasma convection and energetic particle precipitation, can be transposed from the magnetosphere and thus give ground-based support to in-situ magnetospheric observations by spacecrafts. The plasma flow in the polar ionosphere measured with the incoherent scatter radars is a manifestation of magnetospheric convection and the interaction of the solar wind and interplanetary magnetic field with the Earth's magnetosphere. Measurements with the ISR technique thus allow ionospheric processes to be related back to their origin in the magnetosphere and the solar wind. Precipitation of electrons and protons along the Earth's magnetic field lines, which are accelerated in the magnetosphere, and the mapping of the magnetospheric electric field into the polar ionosphere lead to the characteristic visual aurora. Because of the enhancement of the electron density, which accompanies the aurora, these phenomena and their ionospheric environment can be studied in great detail by the incoherent scatter radars with the necessary high temporal and spatial resolution as well as with wide horizontal coverage of a few thousand kilometers and vertical coverage up to more than 1000 kilometers. The location of the EISCAT incoherent scatter radars in northern Scandinavia allows the study of these effects within the auroral oval and into the equatorward part of the polar cap.

There are also phenomena in the polar ionosphere which originate in the lower atmosphere and propagate upwards, such as atmospheric tides and gravity waves. These deposit energy and momentum in the mesosphere and thermosphere and constitute competing effects to the input from the magnetosphere. The relative importance of these upward and downward directed phenomena on the thermosphere and the middle atmosphere is being investigated. Changes in the ionospheric plasma are mutually coupled to the background neutral atmosphere, where particularly the temperature and wind fields become strongly variable. These can be studied by specially adapted ISR techniques optimised for small- and medium-scale phenomena, such as atmospheric gravity waves, which are also be generated in the termosphere by auroral effects.

The Magnetosphere
of the Earth

Global scale phenomena, affected by magnetospheric-ionospheric processes, can be investigated in cooperation with other radars, which is done usually in campaign mode operations and yields essential input to models of the global thermospheric circulation. These phenomena are frequently studied in collaboration with optical and other ground-based instrumentation as well as in-situ observations with rockets and spacecraft (e.g., Viking). The incoherent scatter radar technique thus comprises a helpful and frequently indispensable tool to study the wide field of the polar ionosphere and upper atmosphere and their relations to the magnetosphere, and solar wind, as well as the lower atmosphere.

There exist seven incoherent scatter radars in the world, and EISCAT is one of the highest-standard facilities. The experimental sites of EISCAT are located in Tromsø, Kiruna and Sodankylä in northern Scandinavia north of the arctic circle. They consist of two independent radar systems. The schematic outlines the UHF and VHF radar system at the Tromsø site, which is linked by control and data communication lines to the remote sites.

The UHF radar of EISCAT operates in the 933.5 MHz band with a peak transmitter power of 1.5 MW and 32 m parabolic dish antenna, which can be steered mono directionally. Transmitter and receiver are in Tromsø (Norway). Further receiving sites with similar antennas are in Kiruna (Sweden) and in Sodankylä (Finland), allowing bistatic measurements.

The VHF radar in Tromsø operates monostatically in the 224 MHz band with a peak transmitter power of 1.5 MW and a 120 m x 40 m parabolic cylinder antenna, which is subdivided into four sectors. It can be steered in the meridional plane from 30° south to 10° north of the zenith.

Accumulated operating hours

The operation of a total of 2000 hours per year is distributed equally between Common Programmes and Special Programmes. At present five well defined Common Programmes are run regularly about 30 times per year for 24 or more hours to provide a data base for long term synoptic studies. Three Universal Programmes can be started ad hoc during particular geophysical conditions. A large number of Special Programmes, defined individually by associate scientists, are run to study a variety of particular geophysical events. Some examples of these observations are displayed on the internal pages.

The investments and operational costs of EISCAT are shared between:

Centre National de la Recherche Scientifique (France),
Max-Planck Gesellschaft (W.Germany),
Norges Almenvitenskapelige Forskningsråd (Norway),
Naturvetenskapliga Forskningsrådet (Sweden),
Science and Engineering Research Council (United Kingdom),
Suomen Akatemia (Finland)

EISCAT Scientific Association

Table 1 (cont'd): The EISCAT Leaflet

Internal Executive and Budget Meetings take place twice per year. In these meetings the Director, his Deputy, the Business Manager, the Head of Computer Operations, the Senior Scientist and the Site Leaders discuss and agree upon operational, administrative, personnel and budgetary matters. The spring meeting was at Headquarters and the autumn meeting in Tromsø. The EISCAT Annual Review Meetings usually take place in March. The 1989 meeting was held at Hetta/Enontekiö in northern Finland and was organised by the Sodankylä site staff. The spring Administrative and Finance Committee meeting was held in Hamburg and the spring Scientific Advisory Committee meeting was held before the Fourth EISCAT International Workshop in June in Sigtuna near Stockholm. At the end of September the AFC met at the Tromsø site and the SAC met in October in Kiruna. EISCAT International Workshops are held about every two years and bring together the scientists working with EISCAT to present and discuss their results. The 1989 workshop was organised very effectively by the Uppsala Division of the Institutet för Rymdfysik (IRF, Swedish Institute of Space Physics). About eighty participants attended and listened to almost 70 scientific presentations. On behalf of the host Associate the Council member Professor Bengt Hultqvist made the opening remarks and the EISCAT Director presented an introductory note on 'EISCAT: Progress-Maturity-Evolution'. The workshop participants were honoured by the appearance of the General Secretary of the Naturvetenskapliga Forskningsrådet (NFR) of Sweden, Professor Carl Nordling, as well as several members of the EISCAT Council, SAC and AFC.

In November, the EISCAT Council met at the Rutherford Appleton Laboratory in the United Kingdom and was honoured by the participation at dinner of several representatives of the Rutherford Appleton Laboratory and the Science and Engineering Research Council. During this Council meeting, it was decided that EISCAT should take over the Heating Facility at Ramfjordmoen, which has been constructed and is presently operated by the Max-Planck-Institut für Aeronomie. The scientific expectations of the Heating research are included in a special

report, which was prepared by an active group of scientists using EISCAT and the Heating facility. From the year 1993, EISCAT will own and operate this facility which will allow more combined EISCAT operations during ionospheric modification experiments. Resulting from a proposal by the United Kingdom, plans are also being discussed to add an additional radar, on Spitzbergen, to EISCAT in order to extend the viewing area further into the polar cap. The Scientific Advisory Committee, supported by a special working group, considered the scientific expectations and the potential configuration of such a radar and the Council took opportune note of these plans.

A few staff members left EISCAT in the year 1989; these were: the engineer Arne Björk from the Kiruna site and the tape handler and data analysis operator Dan Lindgren from Headquarters. In the spring, Dr. Cesar La Hoz finished his term as Assistant Director in Tromsø; in his honour, a special colloquium was held at Headquarters in Kiruna. We all acknowledge the important contributions of these persons to the operation of EISCAT. From spring 1989, Dr. Gudmund Wannberg became the Deputy Director of EISCAT and in June 1989 Dr. Anthony van Eyken took the Senior Scientist position and Stefan Heck the Radio-Frequency engineer position at the Tromsø site. Torill Johansen, Inge Marttala, Lena Ståhl and Kari Tuovinen were other staff members who joined EISCAT in Tromsø and Kiruna, respectively. In general, the staffing level has been stable, with 35 persons in post during 1989. The total budget outcome was at a level of 16.72 MSEK, recurrent chapter, and 2.60 MSEK, capital investment chapter (Fig. 2).

I thank Tony van Eyken for compiling and editing this year's Annual Report; it is shorter, and less colourful, than those of recent years but this should not be taken as a sign of reduced operation or scientific output (on the contrary, see pages 13-40 and the 59 papers, and 34 other publications, in the reference lists, starting on page 43). Rather, the reason is a budgetary one since we have to share the costs between this 1989 Annual Report and an EISCAT Brochure, which is being printed at the same time. We hope that both publications provide a suitable and informative overview of recent operations and science as well as the general scope of EISCAT, leading the way into a successful next decade.

Jürgen Röttger

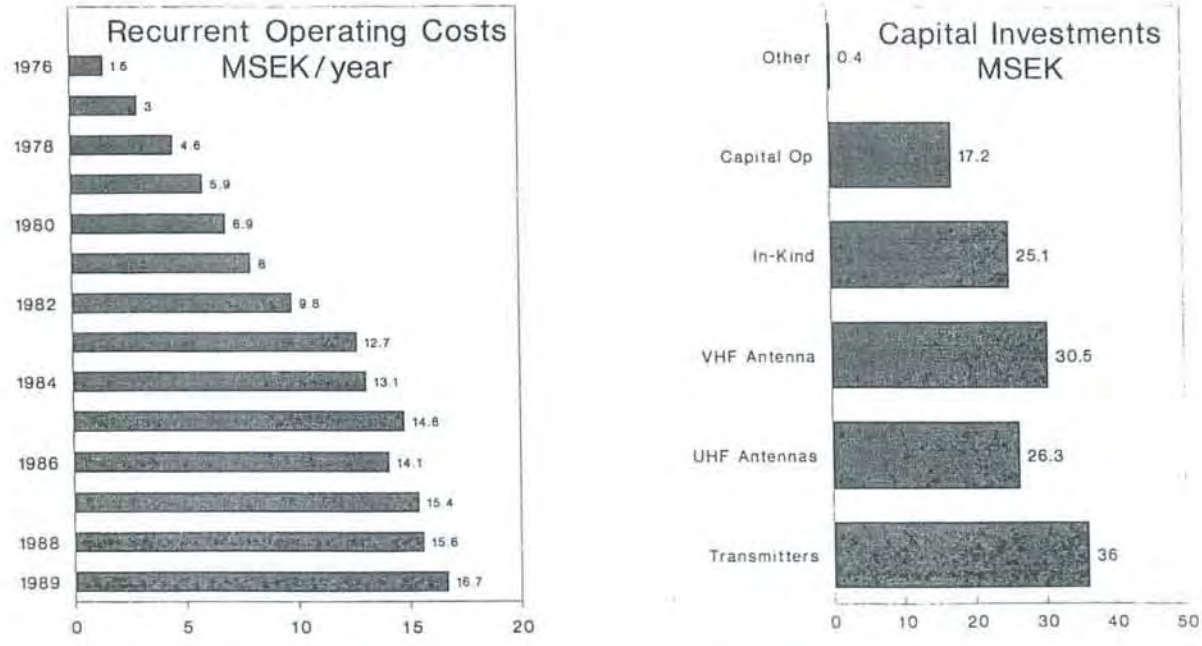

Fig. 2. The yearly development of EISCAT's recurrent budget (left) and the distribution of the accumulated capital investment (right).

EISCAT OPERATIONS IN 1989

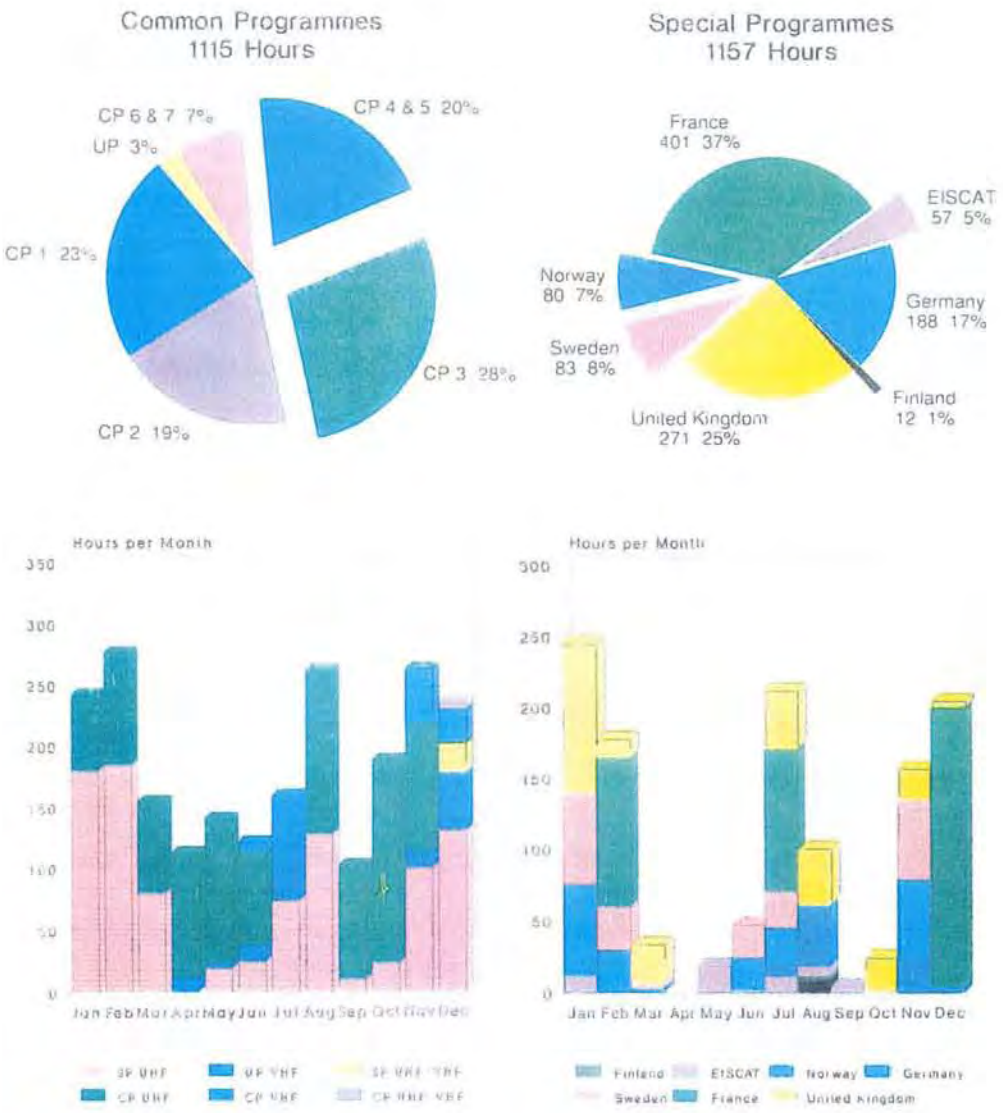

Fig. 3. Total EISCAT Common and Special Programme operations in 1989, and distribution of programme time by month.

EISCAT operations (Fig. 3) throughout 1989 again placed heavy demands on the systems; nevertheless, the diligence and professionalism of the staff at all the sites ensured a very high level of system availability, as revealed by the charts on this page. Activities were almost equally divided between Common Programmes, top left, and Special Programmes, top right. All seven Common Programme modes (see descriptions on page 12) were used this year - though CP-6 only in the form of tests.

Operations were well distributed throughout the year, lower left, though with the usual summer and winter peaks. The welcome appearance of dual radar operations, for both CPs and SPs, in December marks the culmination of much software and hardware development and surely indicates the trend for the future. The seasonal peaks are primarily caused by extensive Special Programme campaigns, lower right. This year, there were several substantial campaigns during the winter months, and a large collaborative Polar Mesosphere Summer Echo study, involving time from several Associates, in the summer. Results from some of these campaigns are described elsewhere in this Report.

COMMON AND UNUSUAL PROGRAMME OPERATIONS AND ANALYSIS

START YY-MM-DD	HH	END MM-DD	HH	EXPT
COMMON PROGRAMME* DATA 1989				
89-01-10	09UT	01-11	23UT	CP-1-I
89-01-31	09UT	02-01	15UT	CP-3-F
89-02-07	09UT	02-08	09UT	CP-1-I
89-02-14	09UT	02-15	17UT	CP-2-D
89-02-21	09UT	02-22	16UT	CP-3-F
89-03-07	09UT	03-08	16UT	CP-3-F*
89-03-28	08UT	03-29	22UT	CP-1-I
89-04-10	10UT	04-13	08UT	CP-3-F*
89-04-25	08UT	04-26	22UT	CP-2-D
89-05-02	08UT	05-03	08UT	CP-1-I
89-05-09	08UT	05-11	08UT	CP-3-F*
89-05-30	10UT	06-04	14UT	CP-5-A*
89-08-01	13UT	08-03	16UT	CP-1-I*
89-08-28	12UT	09-01	16UT	CP-2-D*
89-09-05	10UT	09-06	13UT	CP-1-I
89-09-19	10UT	09-21	14UT	CP-3-F
89-10-02	12UT	10-06	16UT	CP-4-A*
89-10-23	18UT	10-25	14UT	CP-2-D
89-11-14	10UT	11-16	16UT	CP-1-I
89-11-27	10UT	11-29	16UT	CP-3-F*
UNUSUAL PROGRAMME* DATA 1989				
89-03-10	09UT	03-10	17UT	UP-1
89-10-02	10UT	10-02	11UT	UP-1
89-10-20	09UT	10-20	13UT	UP-1
89-10-23	12UT	10-23	18UT	UP-1
89-12-01	09UT	12-01	12UT	UP-1

Table 2. EISCAT Common and Unusual Programme operations and data analysis overview for 1989. Marked entries indicate World Day operations, for which the results have also been sent to NCAR, Boulder.

* OPERATING MODES EMPLOYED IN 1989

Common Programme One, CP-1, uses a fixed transmitting antenna, pointing along the geomagnetic field direction. The three-dimensional velocity and anisotropy in other parameters are measured by means of the receiving stations at Kiruna and Sodankylä (see map, inside front cover). CP-1 is capable of providing results with very good time resolution and is suitable for the study of substorm phenomena, particularly auroral processes where conditions might change rapidly. On longer time scales, CP-1 measurements support studies of diurnal changes, such as atmospheric tides, and seasonal variations. Solar cycle variability will also be studied when sufficient data have been collected.

Common Programme Two, CP-2, is designed to make measurements from a small, rapid transmitter antenna scan. One aim is to identify wave-like phenomena with length and time scales comparable with, or larger than, the scan (few ten km and about ten minutes). The present version consists of a four position scan which is completed in six minutes. The first three positions form a triangle with vertical, south and south-east positions, while the fourth is aligned with the magnetic field. The receiver site antennas make three-dimensional velocity measurements in the E-region.

Common Programme Three, CP-3, is a 10 latitudinal range (in the F-region) with a 17 position scan up to 74°N in a 30 minute cycle. The observations are made in a plane defined by the magnetic meridian through Tromsø and the Kiruna or Sodankylä antenna and is therefore asymmetrical to the F-region.

Common Programme Four, CP-4, covers latitudes up to almost 80°N (77°N invariant latitude) using low elevation, azimuth beam swinging. CP-4 is particularly suitable for studies of high latitude plasma convection.

Common Programme Five, CP-5, has been designed to suit the objectives of lower thermosphere coupling studies. It combines a latitudinal scan with detailed measurements along the Tromsø magnetic field line. The primary aim of this experiment is to observe the dynamics of the neutral atmosphere, while simultaneously exploring the local electrodynamic environment.

Common Programmes One to Five are run on the UHF radar. Two further programmes are designed for use with the VHF system. Common Programme Six, CP-6, is designed for low altitude studies, and Common Programme Seven, CP-7, for high altitude, particularly polar wind, work. CP-7 has been operated several times in 1989, but CP-6 has so far only been run in the guise of UP-1, below, with which it is identical.

Three Unusual Programmes have been defined: UP-1 for D-region observations (widely used this year, on the UHF radar, in connection with Polar Cap Absorption events), UP-2 for auroral arc and related studies and UP-3 for high resolution sporadic E-layer (Es) work. These programmes are started at short notice when suitable geophysical conditions are detected.

MESOSPHERE AND D-REGION

Further studies of polar Mesosphere Summer Echoes (PMSE), which were detected with the EISCAT VHF and UHF radars, yielded some more insight into the characteristics of these echoes. These strong echoes are not due to conventional incoherent scatter, but the final interpretation of the scattering mechanism, and the generation mechanism of the scattering irregularities, causing the PMSE is still undecided. Using multiple beam directions and the newly developed frequency domain interferometry it was found that the scattering irregularities can be localized in thin sheets, less than some hundred meters in thickness; these sheets can be inclined away from the horizontal (van Eyken, C. Hall and Williams; Franke, Hoppe, La Hoz, Rietveld, Röttger)*.

Although such irregularities, which are the cause of Polar Mesosphere Summer Echoes, occur in the same altitudes around 85 km, and during the same summer time period, as noctilucent clouds (NLC), a clear relation between PMSE and NLC has not been found experimentally. The lack of correlation between the occurrence of NLC and PMSE may be explained by the characteristics of the nucleation process, which forms the ice crystals causing the NLC, and other factors that control the visibility of NLCs, such as viewing angle and particle size (Taylor et al., 1989).

It is very evident that there is a pronounced frequency dependence of the PMSE, i.e. the echo intensity is much stronger at VHF than UHF. This was demonstrated by comparing the measurements with the EISCAT UHF and VHF radars together with the 46.9 MHz Cornell University Portable Radar Interferometer (CUPRI) radar, which had been operated in Tromsø in summer 1988. It is thought that more than one scattering mechanism is needed to explain these observations (Röttger, Rietveld, La Hoz, T. Hall, Kelley and Swartz).

Some theories are in preparation to explain the scattering and irregularity generation mechanism. These encompass enhanced turbulence due to super-saturated gravity waves, an increase in the ambipolar diffusion coefficient causing the electron density fluctuations to extend to smaller scales than in the neutral gas (Kelley, Ulwick, Röttger, Inhester, T. Hall and Blix; C. Hall), the formation of electron clouds around charged dust particles enhancing the scatter cross section (Havnes), enhanced electron density gradients which can occur due to increased attachment and recombination or capture of electrons in the presence of thin layers of heavy positive ions (Röttger and La Hoz). The latter three processes work best in a very cold environment such as the summer polar mesopause. More experiments, particularly together with rockets, are needed to understand the mechanisms behind Polar Mesosphere Summer Echoes.

Frequently, pronounced velocity variations are observed in the presence of Polar Mesosphere Summer Echoes and the intensity of the PMSE echo can vary with the same period as the velocity. Fig. 5 shows such an event; immediately below the PMSE layer an atmospheric gravity wave was observed with the same period of 27 minutes. The maximum intensity of the echoes corresponded to the maximum upward velocity of the wave. It was suggested that particle precipitation, adiabatic cooling due to the upward velocity, wave steepening and wave breaking at the mesopause all play a part in causing these events. Also, gravity wave dissipation and breaking can explain why regular wave oscillations, which normally increase exponentially with height, drop sharply in amplitude around 86 km (Williams et al., 1989; Williams and G. Jones).

Energetic solar proton events (SPEs) occur most frequently during the sunspot maximum. These SPEs result in a strong and long lasting D-region electron density in the polar cap, which causes enhanced radio wave absorption known as polar cap absorption (PCA). The present sunspot cycle is at its maximum in the years 1989-1990. Several of these SPEs occurred in the last year and were observed with EISCAT, mostly in Unusual Programme operations.

---

* References given without dates indicate work in progress, or in press. Others can be found in the reference lists, starting on page 43.

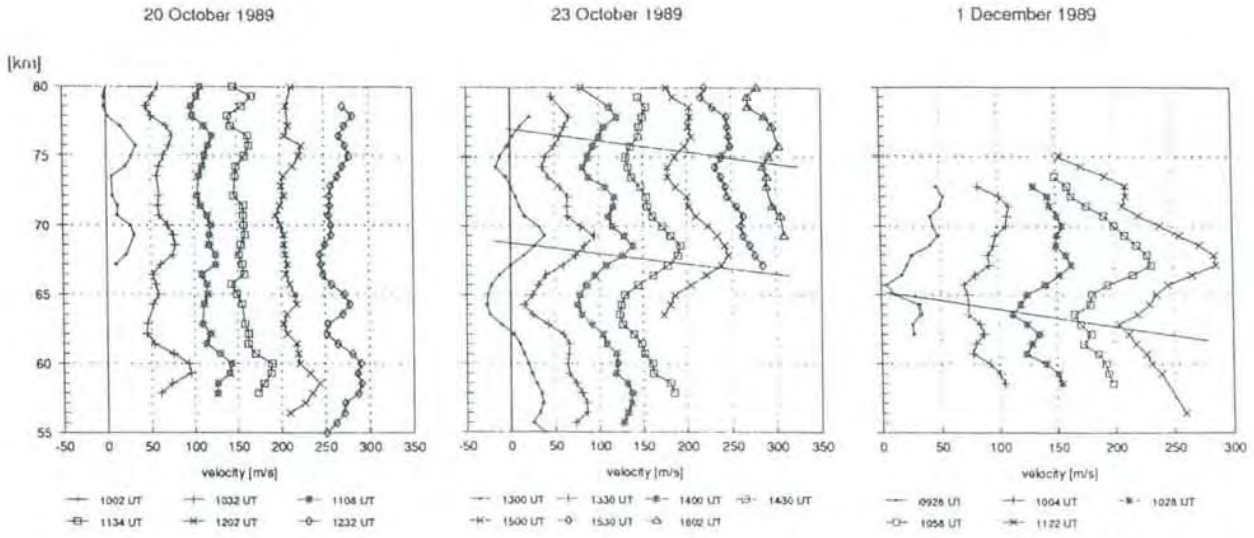

Fig. 4. Northward velocity profiles measured during PCA events with the UHF radar. Each profile is an average over 2 minutes and is offset by 50 m s^{-1} to the right of the previous ones. The sloping solid lines show the descending velocity maxima.

The prolonged D-region ionization during PCA events results in long series of good signal-to-noise ratio data down to altitudes of about 50 km. These data series have also been analyzed to observe long-period waves. In Fig. 4, meridional velocity profiles are shown, which were measured with the UHF radar at an elevation angle of 45°. Clearly, very large velocity amplitudes and vertical wave structures with descending phase can be seen. A colour representation of some of these results appears on the front cover of this Annual Report. The relationship between these strong velocity amplitudes and PCA events needs to be studied as well as whether they are related to 8-10 hour waves or to the semidiurnal tide (Rietveld, Collis and Röttger).

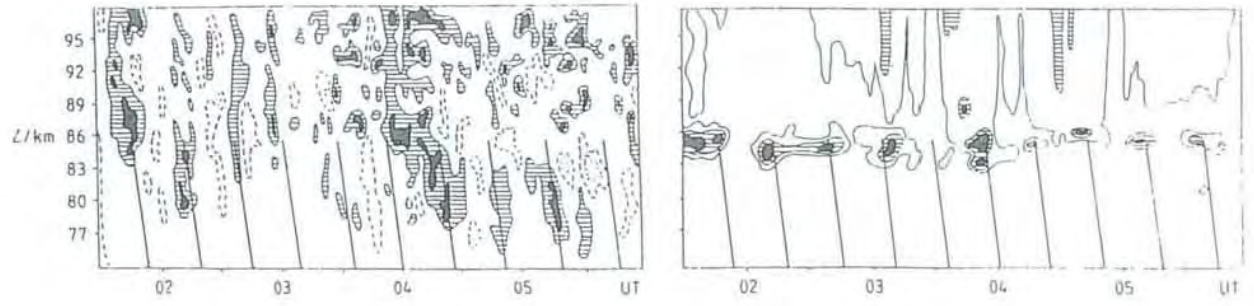

Fig. 5. Height-time contours of echo intensity (left diagram) and vertical velocity (right diagram) during the presence of Polar Mesosphere Summer Echoes measured on 12 August 1988 with the VHF radar. The slanted lines show the phases of maximum upward velocity. The intensity varies over almost two orders of magnitude and the velocity varies between +/- 2 m s^{-1}.

Radar observations during SPEs showed increased electron densities down to 50-55 km, the lowest ionospheric heights from which signals have so far been detected by EISCAT. At these heights the ion chemistry is complex and negative ions form part of the plasma, particularly at night when free electrons can attach to neutral species to form negative ions. Sunlight easily destroys most negative ions and their formation is therefore most pronounced at night. The lack of data in the lower altitudes after 14:30 UT on 23 October (seen on the front cover display) is caused by the reduction of electron density at sunset, even though the ionisation rate due to the incoming protons remained essentially unchanged. Twilight observations are particularly important for studying the behaviour of the negative ion population. Increasing negative ion densities at sunset were detected through the increasing width of the incoherent scatter spectrum as the solar zenith angle increased beyond 90° (Rietveld and Collis).

Fig. 6 shows the diurnal variation of the electron density, measured with EISCAT, and the absorption, measured with riometers at Kilpisjärvi and Kevo. Detailed analysis of the time variation of the electron density indicated that the altitude regions above and below about 68 km were governed by two different mechanisms. Changes above 70 km could be explained by solar UV radiation interacting with high-affinity negative ions (possibly NO_3), whereas below 66 km the temporal variation of neutral oxygen species appeared to play the controlling role (Collis and Rietveld).

Under quiet ionospheric conditions (i.e. without any particle precipitation) the D-region can be modelled since the electrons can then be assumed to be solely due to photo-ionization processes. Using a neutral atmosphere model and an assumed solar flux, the equilibrium profiles of electron concentration can be determined from chemical models. Using a D-region electron density profile measured with the UHF radar, it was shown that a modification of the nitric oxide profile considerably improves the fit to the data. The deduced nitric oxide profiles were used to study the effect of the solar zenith angle. The profiles show peak concentrations between 1.5 and 4.0 10^{15} m^{-3} at 95 to 100 km and about 10^{13} m^{-3} at 80 km altitude. Such values are more representative of previous estimates during disturbed conditions than of the quiet conditions during the EISCAT observations (Burns, Matveinen, Ranta, E. Turunen, and Hargreaves).

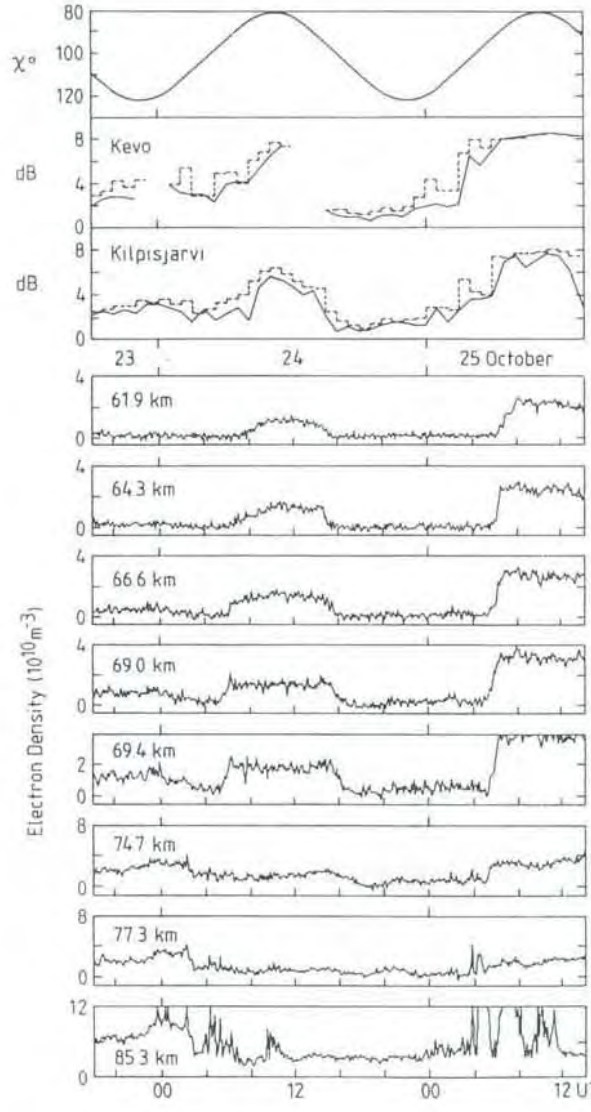

Fig. 6. Time series of electron density, measured with CP-2 on 23-25 October 1989, solar zenith angle (χ) and absorption (dB) during a solar proton event.

Most of these D-region measurements are made with the Barker coded GEN-11 program. The application of this particular modulation scheme leads to range ambiguity effects, which can be minimized by means of special correction procedures (Pollari et al., 1989).

E-REGION STUDIES

Studies of the E-region conductances have continued using CP-1 data. A method has been developed to derive the energy spectra of the precipitating particles from the observed electron density profiles at night-time when no solar ionization is present. This routine is based on a simultaneous fit of a number of 24 ion production profiles, caused by mono-energetic electron beams, to the observed electron density profiles (Brekke, Moen, C. Hall, Pettersen and Hansen).

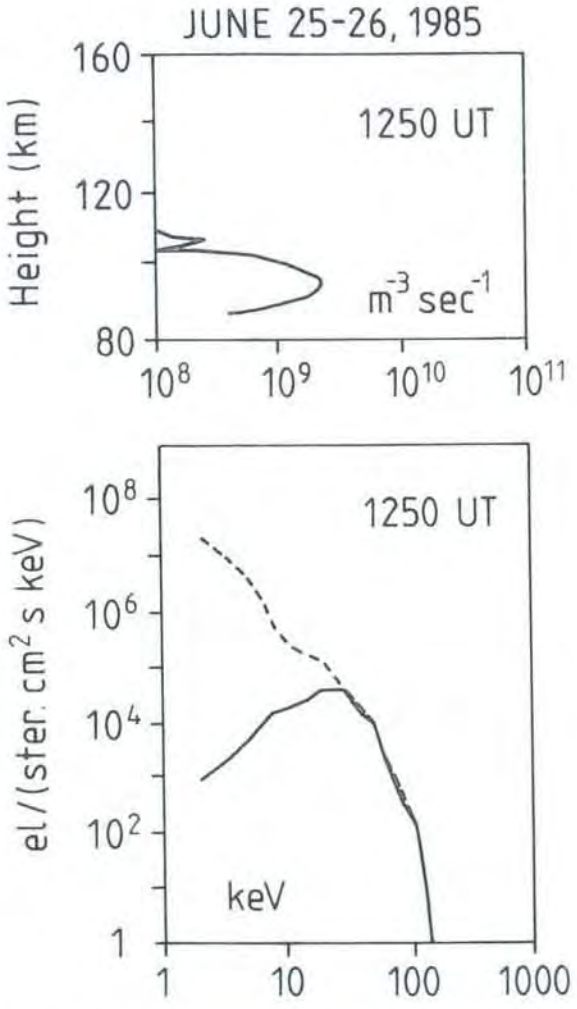

Fig. 7. Upper panel: Particle ionization rate profile during the period 1250 to 1355 UT on 25 June 1985. Lower panel: resultant energy distribution of particle flux (full line) using the ion production rate profiles in the upper panel. The broken line is the energy spectrum obtained using the total ion production rate profile (solar background ionization not subtracted).

An attempt has been made to derive an empirical relationship between the root mean square energy (E_{rms}) of the precipitating auroral particles and the Hall to Pedersen conductance ratio (R). It has been found that for values of E_{rms} less than about 15 keV this relationship can be expressed by an exponential formula as follows:

$$E_{rms} = A \exp (R/B)$$

where A and B are constants derived from the data to be 2.22 +/- 0.30 keV and 1.66 +/- 0.35 keV, respectively. These derived results are in reasonable agreement with Maxwellian energy spectra.

During day-time precipitation events, however, the solar ionization contributes to the conductances as derived from the measured electron density profiles in contrast to the situation at night-time. For such day-time events, a correction has to be made for this background ionization before the routine can be used to derive the energy spectra of the precipitating particles. A method has been developed to achieve this correction and residual ion production profiles for these day-time events are rather height limited and usually situated below 110 km (see Fig. 7). The derived spectra from these profiles are narrow banded with root mean square energies typically larger than 20 keV (Moen, 1989; Brekke, Moen, C. Hall, Pettersen and Hansen).

The Rocket and Scatter Experiment (ROSE) project was a coordinated study of the auroral E-region using rocket-borne instrumentation, EISCAT and STARE (Scandinavian Twin Auroral Radar Experiment). A major scientific objective was to investigate the discrepancy of derived DC electric fields from EISCAT and STARE. EISCAT observed above the rocket trajectory, the common volume being at an altitude of 150 km on the same field line as the rocket apogee, during four ROSE flights. EISCAT determined E-fields above the rocket and at the same time observed the region of E-region instabilities in the Tromsø beam.

In Fig. 8, the series of arrows gives the magnitude and direction of the electric field perpendicular to the magnetic field lines, E_{perp}, as a function of flight time. The rocket data are measured along the trajectory

(northward from ESRANGE) and the altitude is indicated by the dots. The EISCAT measurements are one minute averages. The STARE measurements are attributed to an area at 110 km altitude just below the apogee. The EISCAT and rocket E-fields agree very well, while the STARE results are smaller in magnitude and are rotated, anti-clockwise, by about 15°. The occurrence of AC electric fields or plasma waves is limited to an altitude region between about 90 and 115 km. The width of this region, and the wave activity, increases with DC electric field strength. The lower part of the activity region is dominated by strong low frequency wave fields, presumably caused by gradient-drift instabilities (Rinnert).

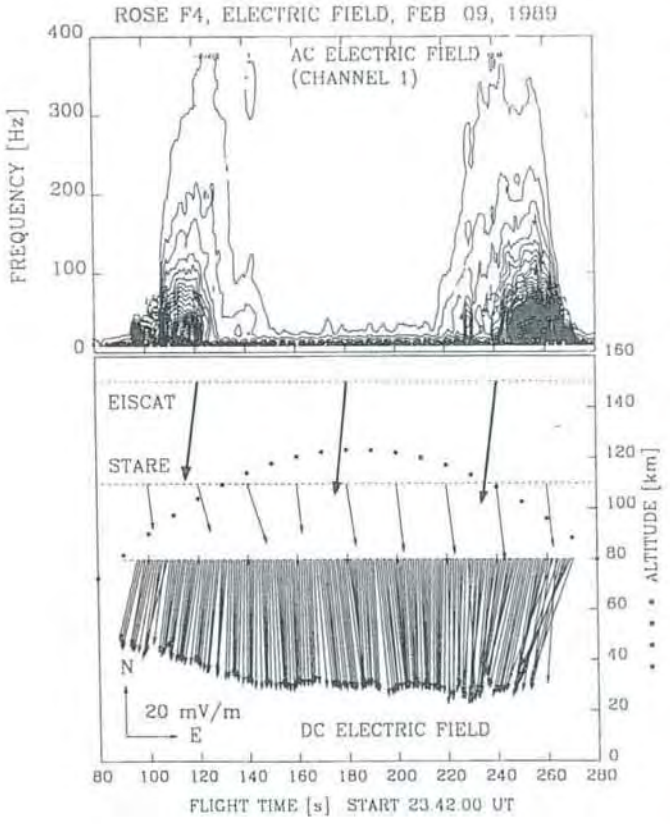

Fig. 8. Electric field measurements, AC and DC, from ROSE payload number 4 and DC electric fields deduced from EISCAT and STARE measurements.

A modified retarding potential analyzer was used on the ROSE payloads for measuring the electron density fluctuations in the range 10-200 Hz which are created by the E-region plasma instabilities. Enhanced fluctuations were observed in a narrow height range, 90-115 km, on the upleg and also on the downleg, in agreement with theory which predicts that the majority of the power will be concentrated in the lower frequency band (10-100 Hz). The relative fluctuations of the electron density, N_e, averaged over all frequencies are in the range of 2-4%. Similar results have been reported by other authors. The instrument was also capable of measuring a relative electron density profile which was calibrated with the help of simultaneously measured EISCAT electron densities (Schlegel).

The optimization of incoherent scatter measurements in the E-region has been investigated. If the power and duty cycle are fixed, then it is possible to improve the detection accuracy by using different kinds of coding. However, the accuracy of the measured autocorrelation function cannot be better than a certain limit, whatever type of coding scheme is used. The accuracy of alternating codes was compared to this limit and a proof of the limiting accuracy based on linear statistical inversion theory has been developed (Lehtinen, 1989).

The fine time and height resolution made possible by the introduction of these alternating codes has led to the most accurate measurements of E-region parameters yet achieved using incoherent scatter radar. For example, during the ERRRIS (E-region Rocket Radar and Incoherent Scatter) campaigns of 1988 and 1989 many hours of observations were made which could be analysed with time resolutions as fine as 45 seconds and height resolution of 4.5 km.

Such data allowed a systematic study of the enhancements in electron temperature, T_e, observed between 100 and 120 km during periods of high electric fields. The fine time resolution demonstrated that the electric field strength varied substantially over short time intervals. On one occasion, for example, the electric field strength along the Tromsø field line increased from 60 mV m^{-1} to 180 mV m^{-1} in about 90 seconds, and fell back to 60 mV m^{-1} in a further 90 seconds. It is clear that previous electric field strength measurements, typically averaged over about five minutes, would misrepresent the true relationship between electric field strength

and T_e enhancement. Special care was taken to identify any spurious data caused by transmitter failure, antenna movement or satellites, and a correction was made for the tidal motions of the neutral atmosphere so that the effective electric field at each height in the E-region could be determined. The observed relationship between T_e and the effective electric field was therefore more reliable than any previously obtained (Fig. 9). This is reflected in the small scatter of the data about the means.

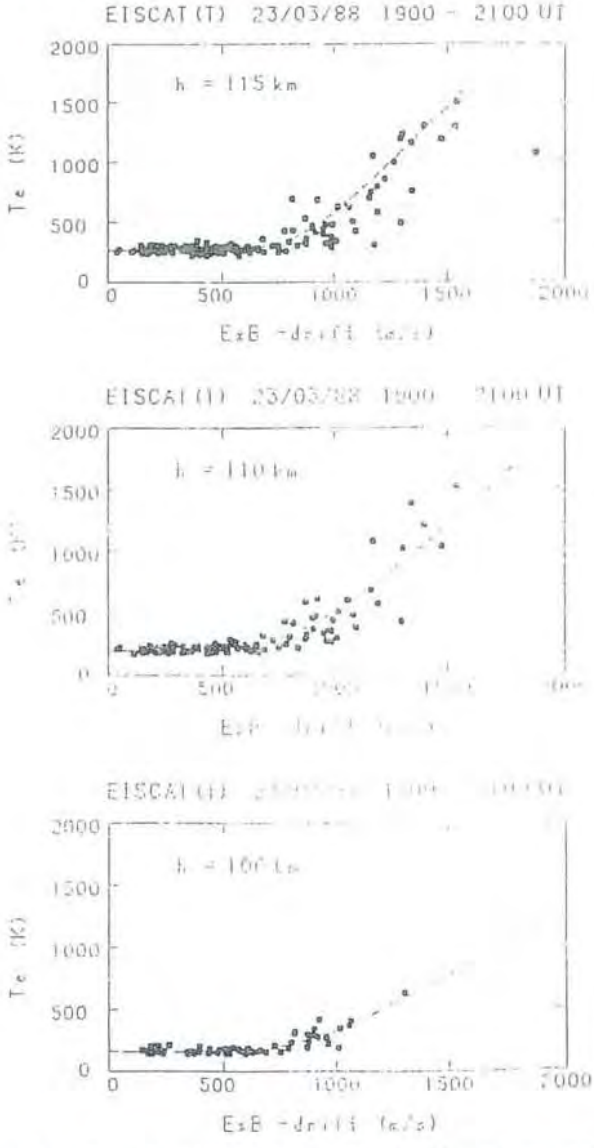

Fig. 9. Electron temperature, T_e, observed at 106, 110 and 115 km, on 23 March 1988, plotted against the electron drift velocity corresponding to the observed electric field. The broken line indicates the relationship predicted by Robinson in 1986, corrected for the estimated neutral velocity at each height (Jones, B., Schlegel, T. Robinson and Häggström).

It was possible to make stringent tests of the various theories proposed to explain electron heating in the E-region, including the model of plasmon-electron interaction proposed by Robinson. Though several of the parameters employed in the model, such as the various coefficients of electron cooling, are not well known, the agreement between the predictions and the observed data is very good (Williams, G. Jones, B. Jones, Opgenoorth and Häggström; Jones, B., Schlegel, T. Robinson and Häggström; Häggström, Opgenoorth, Williams and G. Jones).

Studies of the disturbed auroral E-region were also made using the Dynasonde located at Tromsø. A comparison of the electron densities, N_e, measured by the Dynasonde with simultaneous EISCAT measurements derived from the routine analysis of Common Programme data showed that the concentrations measured by the ionosonde were often a factor of 2 or 3 times greater than the average values given by EISCAT. It is suggested that, under the influence of strong electric fields, large variations exist in the E-region electron concentration with small scale sizes. These lead to biased estimates of N_e, especially when the data are averaged over periods of a few minutes (Wright, Collis, Virdi and Kressman).

EISCAT has made regular observations of plasma velocity, at heights between 101 and 133 km, for many years. After correcting for the effect of the electric field, as measured in the F-region, it is possible to derive the variation of neutral velocity over the same height range. These measurements are best made during quiet magnetic conditions, and 14 days during the period of sunspot minimum between 1985 and 1987 were selected for this purpose. The measured velocities displayed diurnal and semidiurnal tidal oscillations. The diurnal tide showed considerable day-to-day variation in both amplitude and phase. The semidiurnal tide also varied in amplitude but the phase at each height was fairly constant from day to day. Below 120 km the variation of phase with height indicated a dominant (2,4) mode. Above 120 km the variation of phase with height is slower which suggests that at these heights the (2,4) mode is attenuated but the (2,2) mode is still growing with height. (Virdi and Williams, 1989; Williams and Virdi, 1989).

Similar results for the meridional tide were obtained using the ERRRIS database for a period at the beginning of the 1988 which was geomagnetically quiet (Fig. 10). Later in the campaign, however, conditions were disturbed and the tidal modes no longer obeyed the same pattern (Huuskonen, Virdi, G. Jones and Williams).

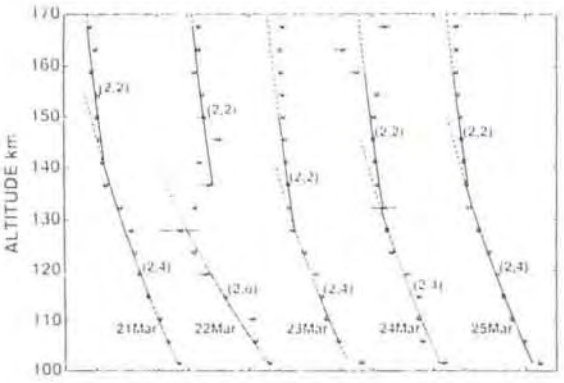

Fig. 10. The fitted phase of the semidiurnal component of the meridional neutral wind on five successive days between 21 and 25 March 1988. The phase profile for the best-fitting mode of the semidiurnal tide is shown in each case (solid line) with the corresponding mode number in parenthesis. The dashed lines are extrapolations of the model profiles beyond the fitted height range (Huuskonen, Virdi, G. Jones and Williams).

Very good measurements of Sporadic E (E_s) layers, and of wave activity in both the E and F-regions, were obtained using the SPORE experiment in the summers of 1987 and 1988 (Lanchester et al., 1989).

The wave spectra shown in Fig. 11 were obtained from the data of 10 July 1987, when strong particle precipitation acted as an irregular energy input, making the wave patterns rather disordered. There is evidence of reflections at certain levels, and of non-linear interaction between a tidal wave and atmospheric gravity waves. Following a strong burst of particle precipitation, an E_s layer formed at 2100 UT; the metal ions appear to have been produced by charge transfer, from molecular ions, rather than by direct ionisation, a tentative estimate of the ambient metal atom concentration being of the order of 10^{11} m^{-3} at 105 km altitude (Nygrén, Lanchester, Huuskonen, Jalonen, T. Turunen, Rishbeth and van Eyken).

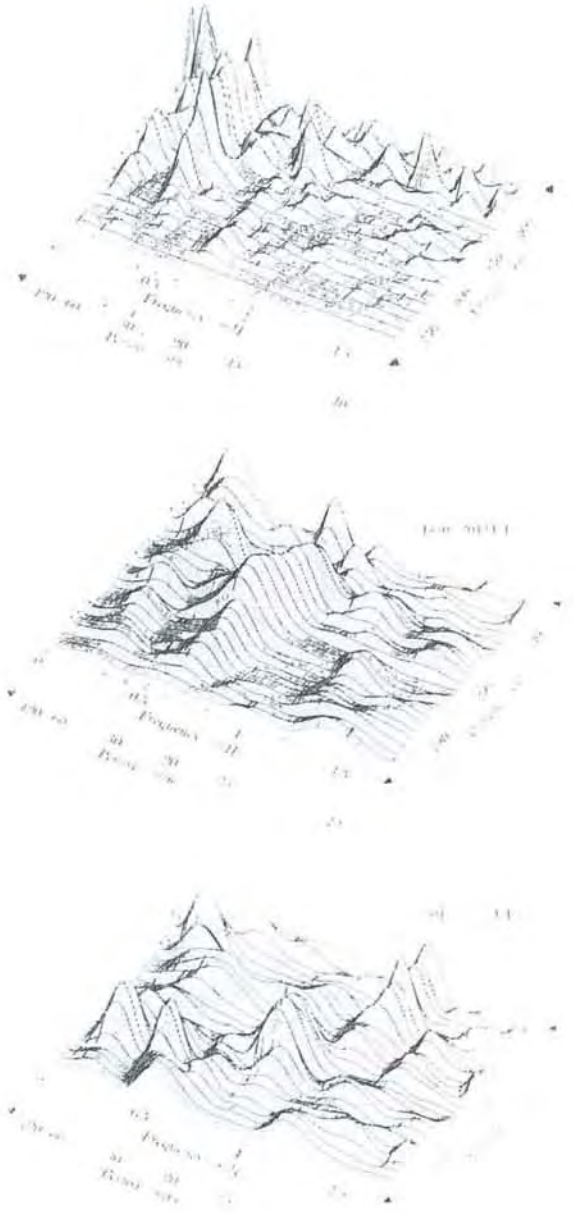

Fig. 11. Power spectra from the F-region (top) and the E-region (lower two) showing the presence of waves of several different periods (Nygrén, Lanchester, Huuskonen, Jalonen, T. Turunen, Rishbeth and van Eyken).

A typical sequential layer event, observed in the afternoon hours, showed the effects of interfering tidal and gravity waves (Fig. 12). The E_s layer was composed of a mixture of light and heavy long lived ions. It eventually dispersed during a rapid upward surge of ion velocity; the atmospheric waves could be followed throughout the E, F1 and F2-regions. It is interesting that the so-called 'corkscrew' mechanism does not necessarily work and, at least in this special case, the E_s layer related to the tidal wave did not transport the metallic ions to low altitudes. The layer was destroyed by rapid upward motions due to changing wind system and the metallic ions were evidently then redistributed to the upper parts of the ionosphere (Lanchester et al., 1989).

The derivation of collision frequencies was further refined using velocity measurements in two directions. Height profiles of two ion velocity components are measured sequentially in vertical and eastward directions and the electric field determined from tristatic velocity observations. The collision frequency is then found by solving the momentum equation. Using incoherent scatter data from August 1985, it was found that the usual model values of collision frequency might be too low. Practically all the high spatial resolution data available in the EISCAT database was used in a further study of collision frequencies. The results indicate that the MSIS-86 model gives correct collision frequencies for July, but underestimates them for February and August. Temperature observations in the E-region show event-to-event variations which exceed those predicted by the MSIS-86 model. The electron and ion temperatures are about equal at 110 km altitude, but in a narrow region above 110 km the ion temperature slightly exceeds the electron temperature (Nygrén et al., 1989; Huuskonen 1989).

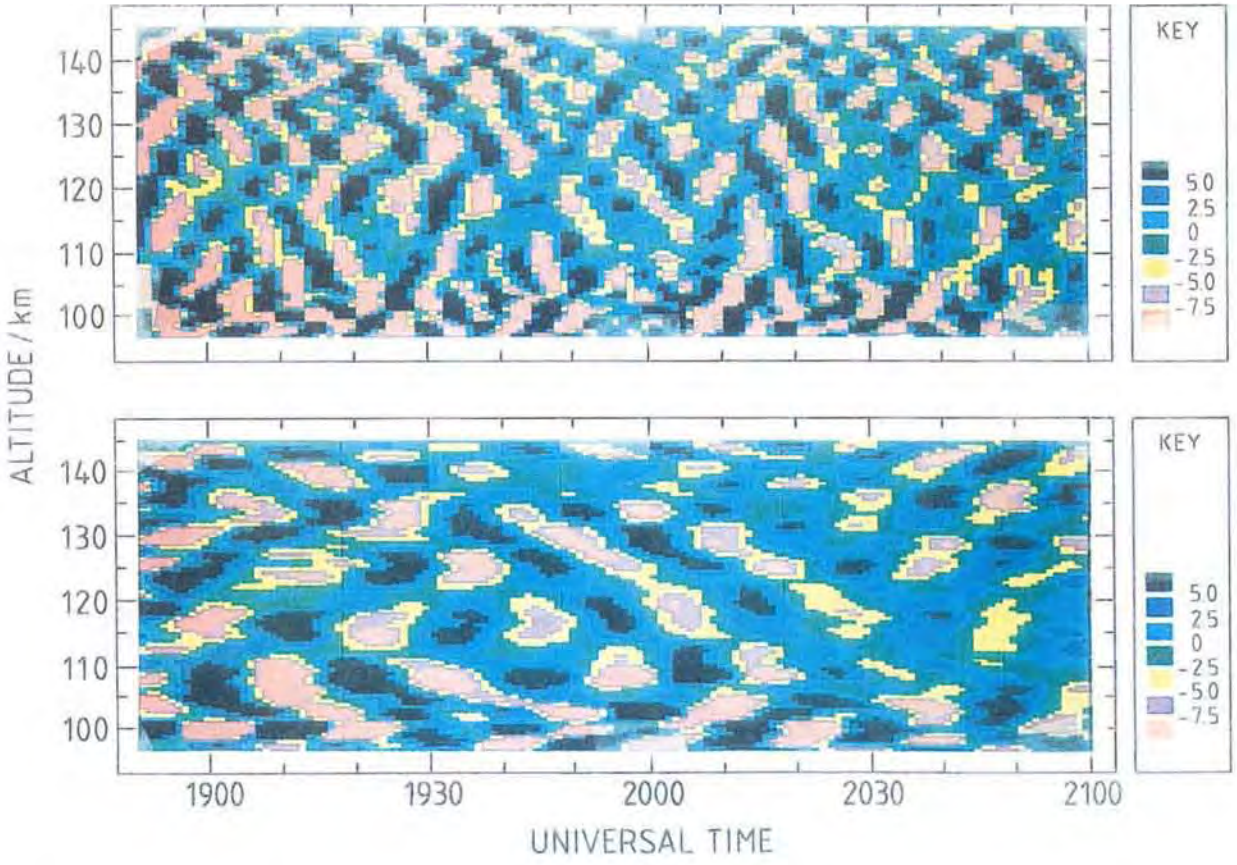

Fig. 12. Interference effects caused by gravity waves propagating in the E-region. The diagrams are produced by filtering the derived velocity fields with bandpass filters centred on gravity wave frequencies revealed by a separate spectral analysis.

AURORAL ARCS

The UP-3 code was used to observe thin ionization layers during pulsating auroras at the same time as the CUPRI radar detected extremely intense backscatter echoes with large Doppler shifts. Such echoes could be produced by current driven, collisional, electrostatic ion cyclotron waves, but other possible mechanisms cannot be discounted. Ion temperature enhancements of up to 100 K have also been observed at altitudes close to and even below 110 km, indicating that extreme heating processes take place within or near these thin ionization layers. An equivalent electric field of 200-300 mV m^{-1} would be required to produce the observed ion temperature enhancements, but EISCAT detected convection fields no greater than 10 mV m^{-1} on these occasions (Fig. 13).

The current hypothesis is that a beam-plasma instability might be responsible for both the thin layers of ionization and the luminosity, the ionization being caused not by precipitating particles but by suprathermal ionospheric electrons, accelerated by instability generated ion cyclotron, and possibly ion drift, waves.

E-region measurements made with 100 ms temporal resolution and 1050 m spatial resolution were compared with optical data. Electron densities calculated from the optical measurements correlated well with the true electron densities measured by the EISCAT UHF radar at 110 km altitude. Auroral and electron density pulsations were observed to occur together. During these pulsations, the enhanced electron densities below 100 km could be caused by two different Maxwellian distributions with energies of about 2 and 10 keV (Kaila et al., 1989, Kaila and Rasinkangas, 1989).

As mentioned earlier, short lived intensifications of the auroral zone electric field have been found to be much more common and intense than previously suspected. Most of these intensifications are associated with the passage of auroral arcs, correlating particularly with their leading edges. Enhancements of the electric field to values about 100 mV m^{-1} on the equatorward edge of evening sector arcs and on the poleward edge of morning sector arcs are, in fact, very common. It appears that the sharpness of the features (several 10 km), and low electron densities in the affected regions, effectively concealed them from radar experiments less optimized than the alternating code techniques now used. Such electric field enhancements outside auroral arcs had earlier been reported only sporadically by rocket studies and seldom included in theoretical or statistical models of auroral arc electrodynamics. The electric field enhancement outside many auroral arcs is probably strongly dependent on ionosphere-magnetosphere interactions. If the configuration of the ionosphere-magnetosphere coupling allows a complete cancelling of meridional currents within the arc, by polarization effects, the field enhancement is not observed. However, when considerable field-aligned currents exist at the arc edges, an electric field enhancement at one edge is a natural consequence of current continuity in the ionospheric and magnetospheric portions of the three-dimensional current system (Opgenoorth, Häggström, Williams and G. Jones).

F-REGION STUDIES

Simultaneous EISCAT and Fabry-Perot Interferometer (FPI) measurements have been used to derive the ion-neutral collision frequency in the high-latitude F-region. It was found to be consistently lower, by a factor of about 2 to 3, than the currently accepted values, a result apparently at variance with similar measurements at Arecibo which suggest an increase in the collision frequency. Standard methods were used to derive the thermospheric winds from the radar data and these were compared with the actual measured winds. First order agreement was quite good but large experimental errors make a quantitative comparison very difficult, and such methods should be used with caution. An analysis of the errors associated with this method suggests that it is very difficult to derive neutral wind vectors from radar data at EISCAT's latitude (Farmer, G. Jones, Williams, Moffett, Samson, Horne, Rycroft, Lester and McCrea).

Coordinated observations by the EISCAT radar and the MICADO Michelson interferometer, located in Sodankylä, were conducted for the first time during the winter of 1988-1989.

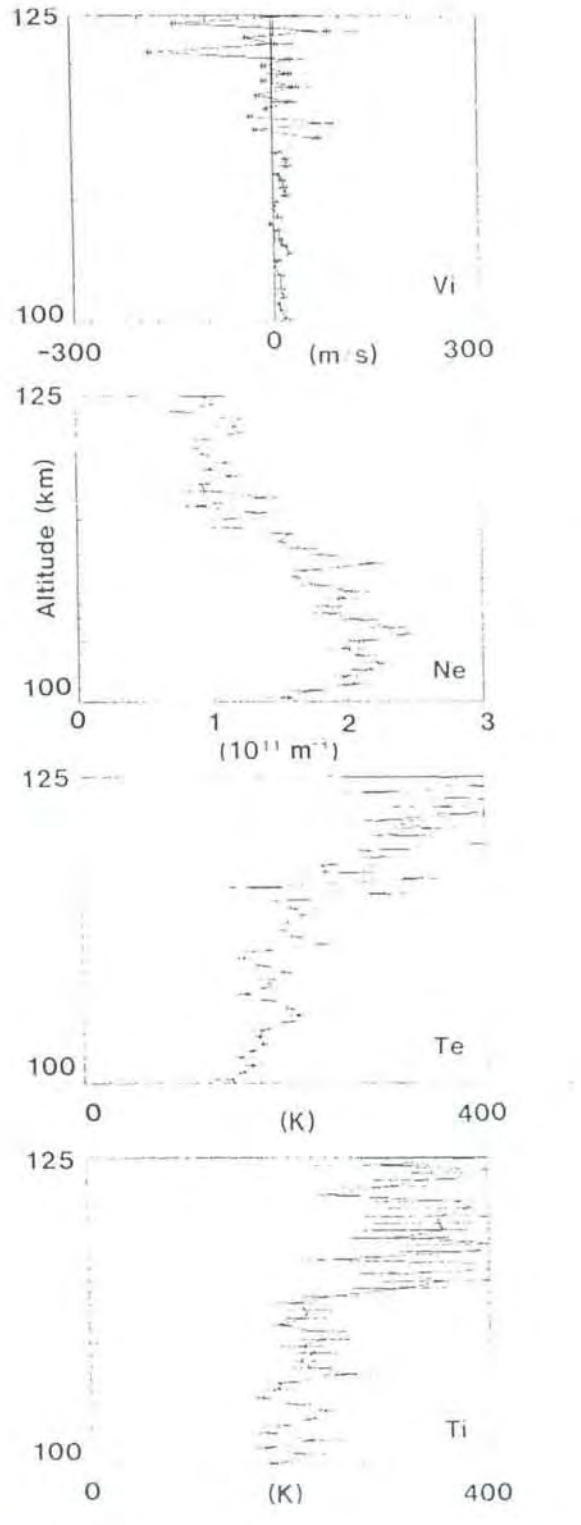

Fig. 13. E-region altitude profiles of field-aligned ion velocity (positive upward) electron density, and electron and ion temperatures derived from UP-3-like data taken at 0341 UT on 3 March 1988. Two or three thin ionization layers can be seen (second panel) with associated enhancements of about 50-75 K in both electron and ion temperature (lower panels).

MICADO measurements of neutral temperature and wind were made using the red O1D line in the F-region thermosphere. The comparison was conducted between the meridional component of the neutral wind measured by MICADO and that calculated using EISCAT data for vertical ion drift, electron density and electron and ion temperatures. It was found that, during active periods, the vertical neutral wind measured directly by the interferometer should be included in the calculation of the meridional neutral wind from EISCAT data. During quiet periods however, when the vertical neutral winds are small, the comparison could lead to an estimate of the O^+/O collision frequency (Thuillier, Lathuillère, Herse, Senior, Kofman, Duboin, Alcaydé, Barlier and Fontanari).

In order to fit incoherent scatter spectra for ion composition, it is usually necessary to assume that the different ion gases have the same line-of-sight temperature. The discovery of anisotropic, non-Maxwellian plasmas means that this assumption is only valid for one beam angle to the magnetic field, 54.7°. Observations of a strong heating event at this aspect angle have shown that, within two minutes of the onset, the ion gas at 275 km is converted from predominantly O^+ to predominantly molecular ions.

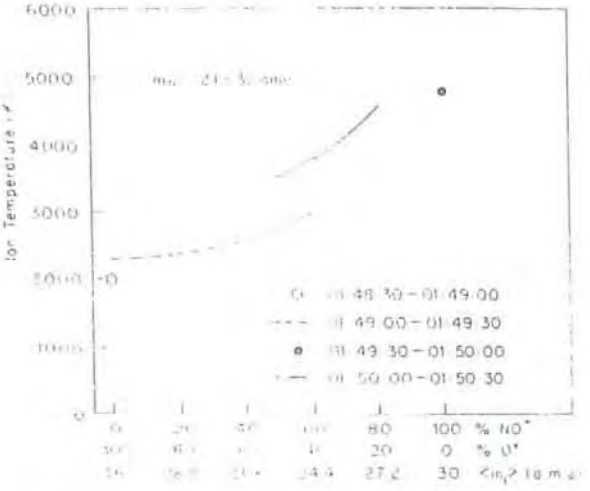

Fig. 14. Ion temperature as a function of ion composition for a major ion heating event on 16 December 1988. Conversion from predominantly O^+ ions to predominantly molecular ions occurs as the ion temperature rises from 2000 K to 5000 K within one minute (Winser, Lockwood, G. Jones, Rishbeth and Ashford).

The data analysis allows for the distortion of the distributions of line-of-sight velocity for the two separate ion populations. The ion composition is computed in two ways: first by fitting synthesized spectra for a two-species non-Maxwellian ion gas to the observed spectra; and second, by defining the mean ion mass required to make the observed ion temperature (which is directly measured at the aspect angle used) consistent with a simplified form of the ion energy balance equation.

Fig. 14 shows the ion composition as a function of ion temperature at the peak of the heating event, derived using the second of these methods. In each post-integration period, the data point is in general somewhere on a line determined by non-Maxwellian fits to the observed spectrum. The limits of that line are set by the ion energy balance equation, using the range of assumed mean neutral masses 21-32 amu (if those limits are close together the line is plotted as a point). For some periods there is a range of values, which reflects uncertainty in the assumed mean mass of the neutral gas, but the observed spectrum width constrains the true point to lie on the segments shown.

It can be seen that, irrespective of the neutral mass, a clear conversion to predominantly molecular ions occurs as the ion gas is heated. Such a complete conversion to a molecular ion gas does not appear to be in agreement with published rate coefficients for the relevant chemical reactions (Winser, Lockwood, G. Jones, Rishbeth and Ashford).

Theoretical collision models predict anisotropic ion temperatures if there is a nett drift velocity between the ions and the neutrals. Five events with relatively sudden and strong increases of the ion drift perpendicular to the geomagnetic field, found in EISCAT CP-1-F data sets, were analysed to investigate the anisotropy and collision process. In a statistical analysis of these events (Fig. 15), the ion temperatures and ion drift velocities from the F-region common volume, at 312 km altitude, were correlated. Because of the CP-1-F geometry and because the ion drifts remained below 1500 m s^{-1}, a bi-Maxwellian was assumed to be a good approximation of the ion velocity distribution and O^+ to be the dominant ion at the F-region maximum. For a theoretical description of the anisotropic ion heating, new expressions for a multi-component neutral background, for arbitrary directions of observation and for an effective central force appropriate to the collision process were calculated. The drift dependence of the ion temperature (derived from the statistical analysis of the Tromsø, Kiruna and Sodankylä data) was in good agreement with the theoretical curves for a bi-Maxwellian distribution of O^+ drifting in a neutral atmosphere consisting of 80% O and 20% N_2 (MSIS-86), with resonant charge exchange collisions between O^+ and O and polarization interaction between O^+ and N_2. There was no indication of NO^+ dominance at the F-region maximum during these events (Glatthor and Hernandez, 1989).

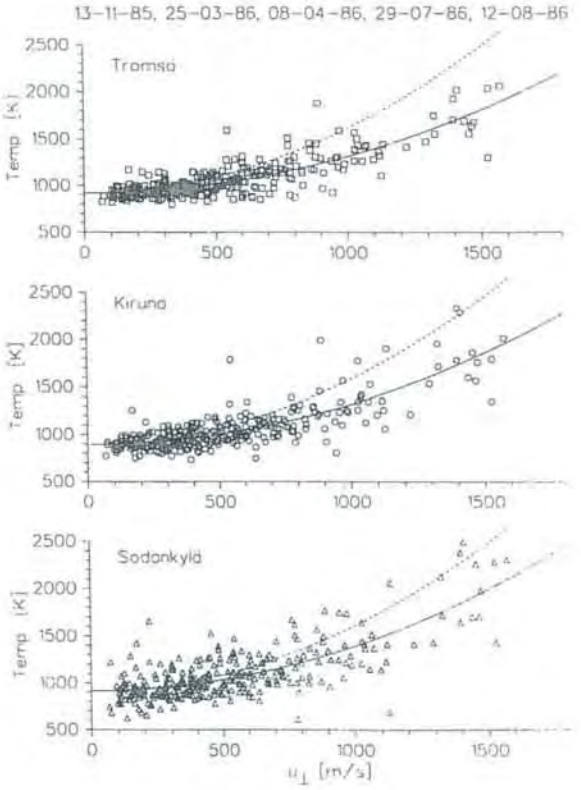

Fig. 15. Ion temperature at 312 km altitude as a function of ion-neutral drift perpendicular to the geomagnetic field, with fitted curves (solid) and theoretical curves for Maxwellian (dashed) and bi-Maxwellian (dots) ion velocity distributions.

PLASMA-D is a combined ion line/plasma line program which uses the CCD spectrum analyzer for the plasma line measurement

and the correlator for ion line data. The results have been used to derive O^+ composition profiles in the F-region between 200 and 250 km by the technique introduced by Bjørnå and Kirkwood (1988). The spectrum analyzer provides plasma lines with improved altitude and frequency resolutions, which is important for the derivation of accurate composition profiles. The O^+ content by this method applied to quiet summer-time data was generally lower than predicted by the EISCAT composition model, with the most significant deviations at the upper altitudes (Fig. 16). The electron temperatures derived using the composition model are underestimated by up to 15% (Fredriksen and La Hoz).

Over 100 cases of ion-frictional heating have been identified from a total of 1250 CP-1 and CP-2 observations. The temporal distribution, Fig. 17, has a peak near magnetic midnight with approximately equal distribution between the regions of eastward and westward ion drift. A close connection was noted between frictional heating and the presence of auroral boundaries, implying that auroral precipitation may be important in determining the structure of frictional heating in the midnight sector (McCrea, Lester, T. Robinson, Wade and T. Jones).

Since the ion thermal velocity distribution is anisotropic, so too is the F-region ion temperature. Ion temperatures parallel and perpendicular to the magnetic field are determined by temperature partition coefficients β_{para} and β_{perp}. By examining the response of T_i parallel to the magnetic field to increasing plasma velocity perpendicular to the field, estimates were made of β_{para} and β_{perp} for the F-region and the variation of β_{para} with height was examined (Fig. 18). In the upper F-region the calculated values of β_{para} agree with those expected for resonant charge-exchange collisions, which are expected to dominate at these altitudes. A persistent increase in β_{para} with height was established, which is believed to be due to the increasing influence of ion-ion collisions, which act to decrease the anisotropy of the ion-thermal distribution and increase the field-parallel component of T_i. The influence of the ion-ion collision frequency on β_{para} introduces a temperature dependence in the partition function whose importance had not been recognised previously.

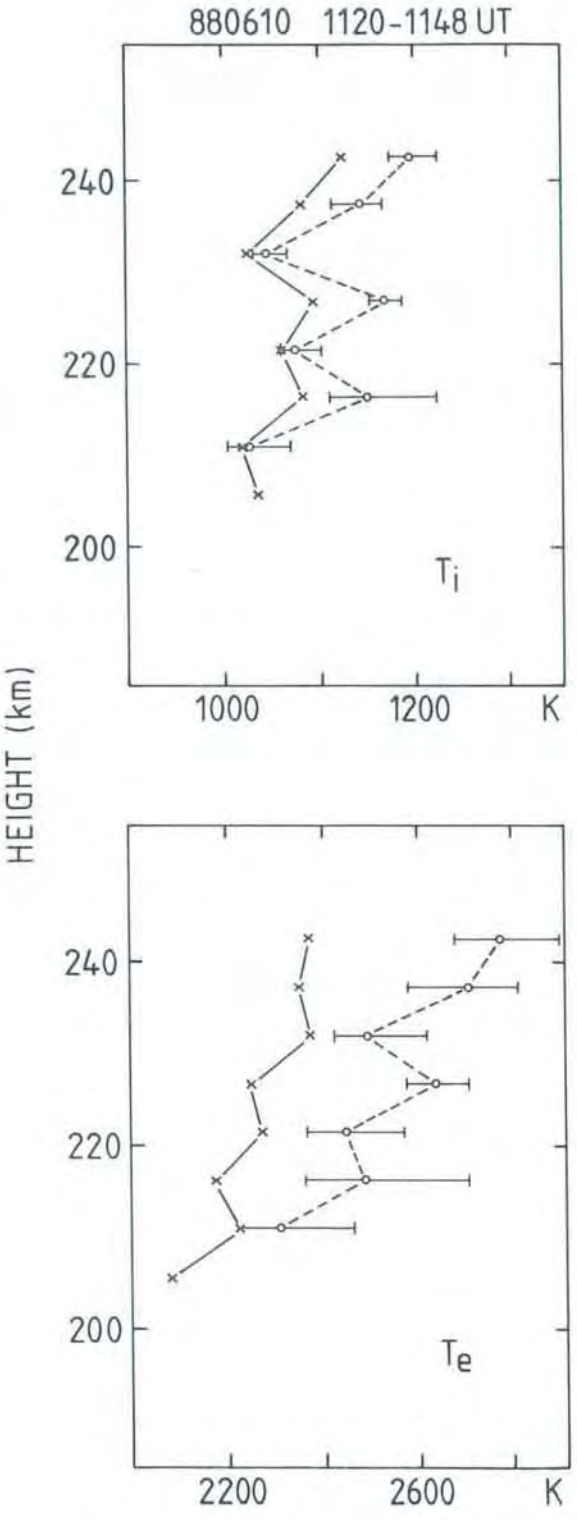

Fig. 16. T_i and T_e from a combined ion line/plasma line fit (dashed curve), compared to temperatures derived from a standard ion line fit using the EISCAT model composition (full curve).

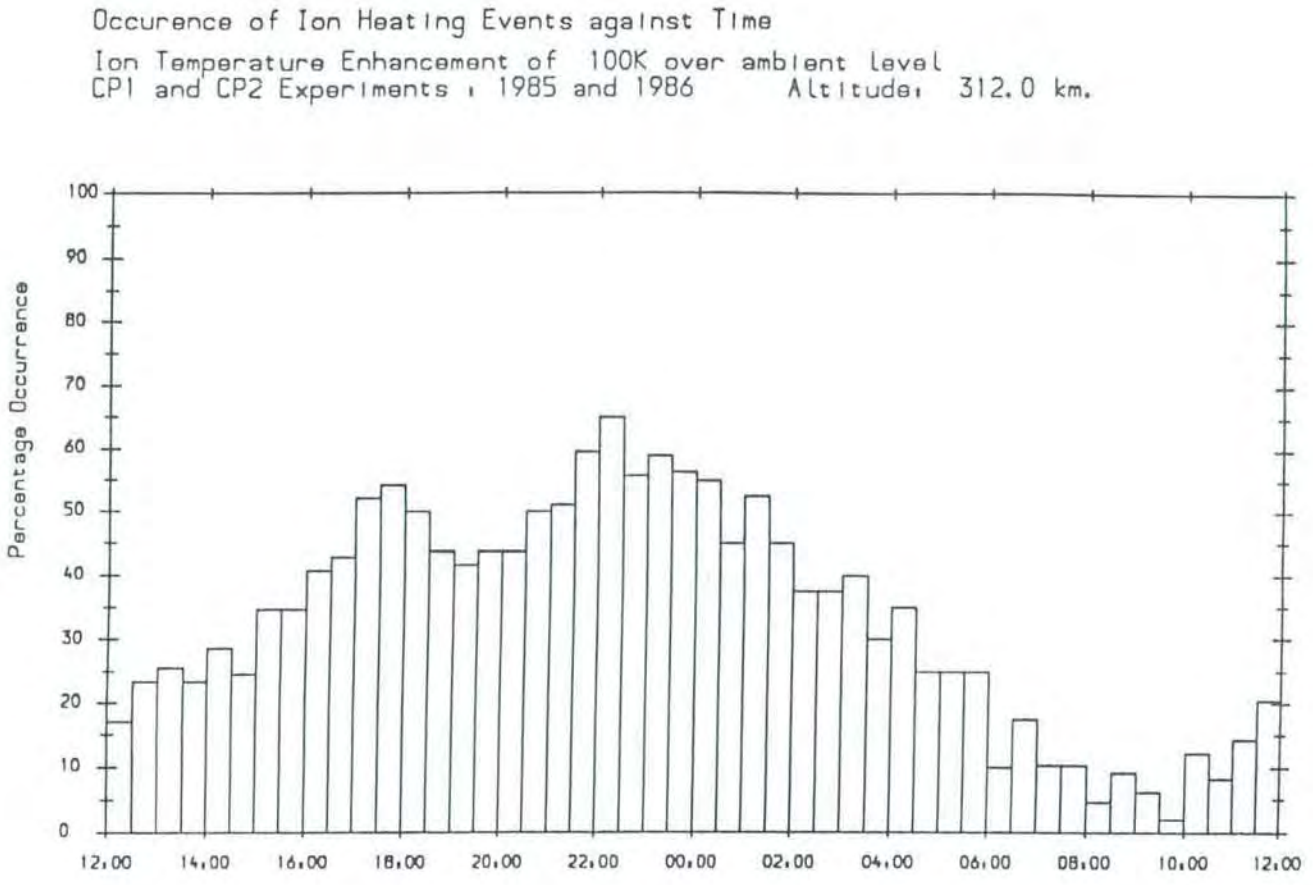

Fig. 17. Percentage occurrence of ion heating events, as a function of UT, for CP-1 and CP-2 observations during 1985 and 1986 (sunspot minimum).

Strong upward ion flows in the high F-region have been found to be associated with strong electron heating during low energy particle precipitation. Continued work on enhanced electron temperatures in the topside ionosphere has resulted in a fundamental change of view regarding the electron energy budget during active aurora. According to earlier understanding, strong convection electric fields and collisional heating by precipitating particles (mainly via secondaries) can account for the total electron heating in the topside ionosphere even during disturbed conditions. However, a detailed investigation of EISCAT data combined with theoretical simulations of topside heating by particle precipitation has shown that such mechanisms do not account fully for the observations. (Wahlund and Opgenoorth, 1989; Lilensten, Fontaine, Kofman, Lathuillère, Eliasson and Oran).

Fig. 19 illustrates the good correlation found between strong enhancements (up to 6000 K) of T_e in the upper F-region (above 300 km) and enhanced electron densities in the lower F-region. The altitude just below 200 km corresponds to auroral precipitation at energies of the order of a few 100 eV. A detailed analysis of T_e altitude profiles shows that the main heat source is located above 300 km, and often even above the maximum observation altitude of 450 km. It is therefore unlikely that the electron precipitation is directly responsible for the observed temperature increase. On the other hand, satellite and rocket observations at altitudes below 1000 km indicate a good correlation between low energy particle precipitation and plasma waves in the upper hybrid band during active conditions.

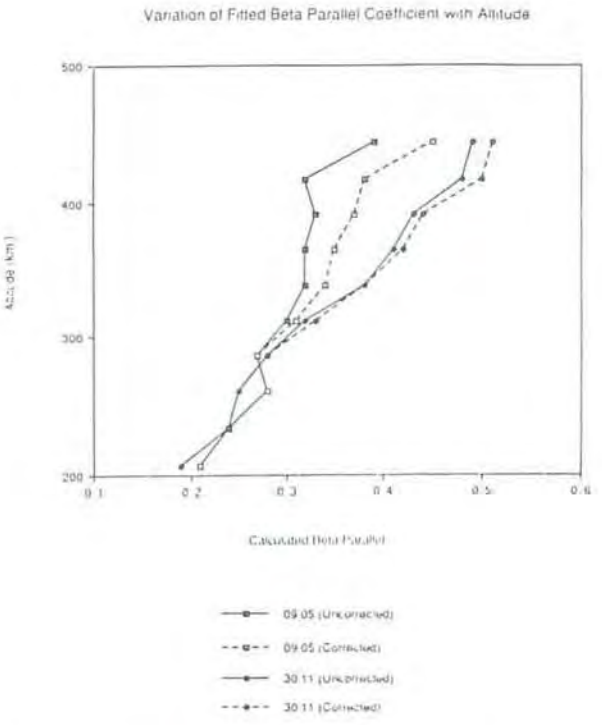

Fig. 18. The altitude variation of β_{para} for two days. The dashed lines include a correction due to the ion-electron heat flux during ion heating events caused by the higher electron temperature.

The amplitude of these waves is commonly found to be in excess of 50 mV m^{-1}. Such waves could easily provide the required heating rates to produce the T_e altitude distributions observed with EISCAT, even when anomalous collisions are included (Wahlund and Opgenoorth, 1989).

During disturbed conditions the temperature of electrons in the F-region above EISCAT is affected by several factors including solar illumination, particle precipitation and ionospheric convection. During sunspot minimum, however, conditions are frequently very quiet and electron concentration and temperature depend only on the solar flux and the ratio of molecular nitrogen to atomic oxygen. As this ratio increases, the rate of production of photoelectrons by the ionisation of N_2 increases, but at the same time the O^+ recombination rate increases such that the concentration of thermal electrons decreases. As a result, there is an anti-correlation between electron temperature and electron concentration, with the exact relationship being controlled by various cooling mechanisms, including Coulomb exchange, and the excitation of the fine-structure energy levels of oxygen and the vibrational states of nitrogen.

By modelling the full energy balance of the thermal electrons, including 16 different cooling terms and the effects of heat conduction, the value of T_e under quiet conditions can be predicted from the observed values of electron concentration and 10.7 cm solar flux.

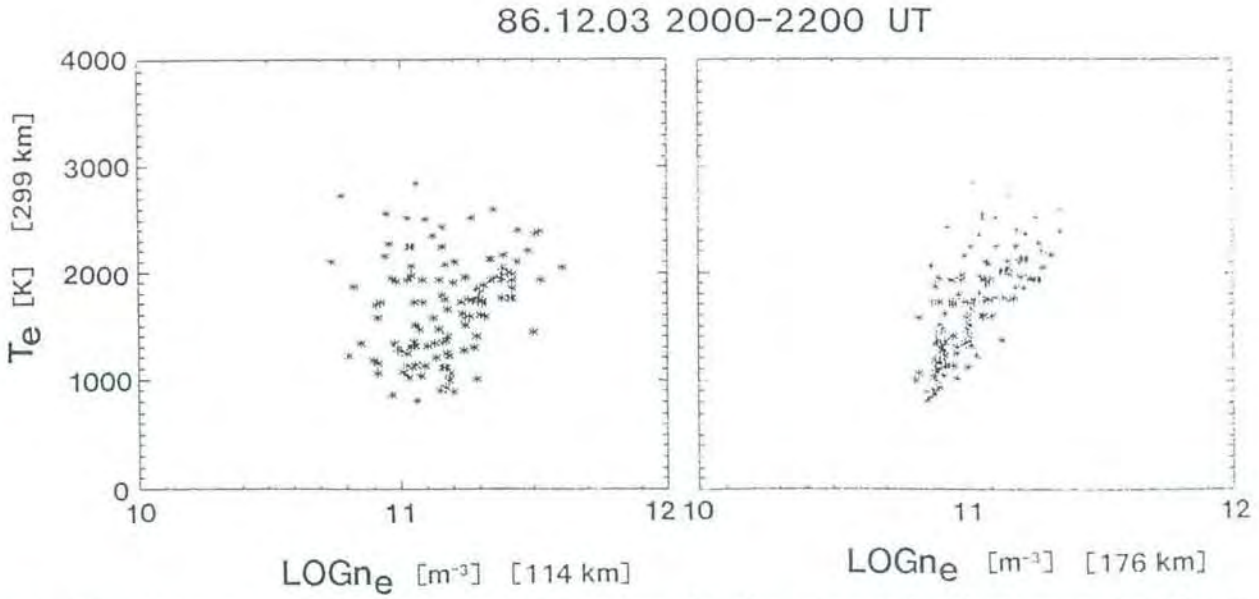

Fig. 19. Electron temperatures at topside F-region altitudes compared with electron densities at E-region (left panel) and lower F-region (right panel) altitudes.

The correlation between the predicted and observed values of T_e is over 90% and the agreement usually lies within the accuracy of observation (Fig. 20). However, at the onset of magnetic activity following a long quiet period, the predicted and observed values of T_e begin to diverge (Breen, Williams and Davda).

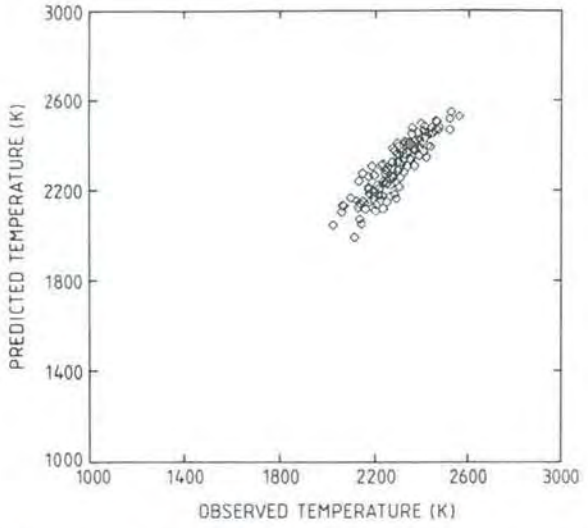

Fig. 20. Comparison of predicted and observed values of T_e, for the height range 260-325 km, during quiet periods on 15 days (Breen, Williams, and Davda).

A statistical study of height-integrated conductivities, derived from EISCAT CP-3 data recorded between June 1984 and November 1987, has been undertaken. The solar-induced component of these conductivities has been modelled as a function of the solar zenith angle; it can be approximated by a linear function of the cosine of the solar zenith angle. The comparison between the particle-precipitation-induced component of the conductivities derived from EISCAT data and the statistical conductivity models of Hardy et al. (1989), derived from DMSP satellite electron precipitation data, show good agreement in the morning sector, but a discrepancy of about 30% in the evening sector, when EISCAT conductivities exceed those of the Hardy et al. models. This discrepancy can be explained by ion precipitation, which was not included in the Hardy models, which is at least qualitatively intense enough in the evening sector, in terms of flux and energy, to ionize the F-region (Senior, Lilensten, Fontaine).

The terrestrial ionosphere is a major source of plasma (both heavy ions and protons) for many regions of the magnetosphere, and EISCAT has played a major role in studying the thermal ion upflows in the ionosphere which are required to supply this plasma. A statistical survey of data taken during CP-1 experiments has revealed that large upflows (and downflows) are a common feature on the geomagnetic field line through Tromsø. Fig. 21(a) shows the percentage frequency occurrence of upflow 'events' as a function of UT, where an event is defined as an upward velocity exceeding 100 m s^{-1} or an upward flux greater than 10^{13} m^{-2} s^{-1} (i.e. an order of magnitude greater than the classical polar wind flux of light ions at greater altitudes).

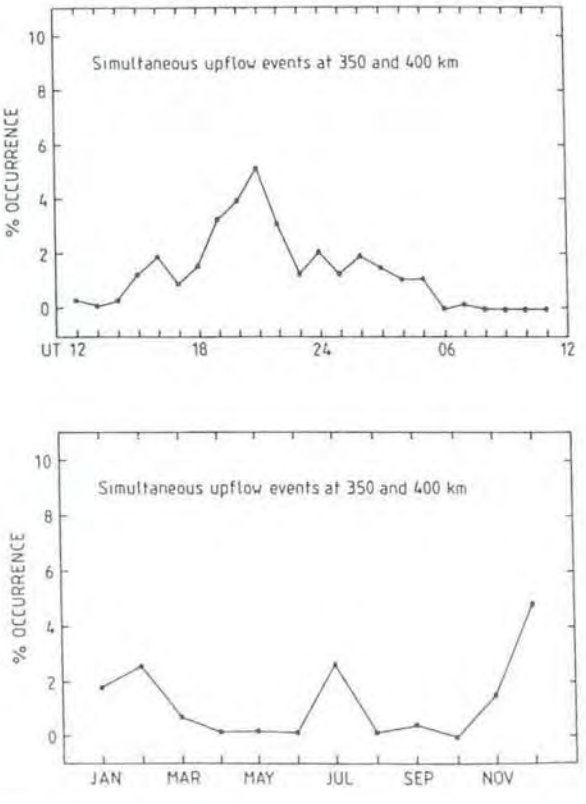

Fig. 21. The occurrence probability of large field-aligned upflow events (velocity > 100 m s^{-1}, or flux > 10^{13} m^{-2} s^{-1}) in 3 years of CP-1 data (1985-1987), as a function of (a) UT and (b) Month (Keating, Winser, Lockwood, Mulligan and Doyle).

The largest probability of such an event occurs near 21 UT, around the time Tromsø passes through the Harang discontinuity.

Fig. 21(b) shows that such events are much more likely to occur in winter (the second peak in summer in fact arises entirely from one very disturbed period in July 1987). These upflows are correlated with increases in F-region ion temperature, which are often seen in association with changes in the field-perpendicular convection, as might occur during the passage of a convection shear through the radar beam (Winser et al., 1989; Keating, Winser, Lockwood, Mulligan and Doyle).

A series of five nights of measurements of the topside ionosphere with the VHF radar in July-August 1988 was used to study the vertical transport of O^+ and H^+ ions, and the resulting exchange of ion species between the ionosphere and the magnetosphere. It was possible to deduce ion densities and composition, ion and electron temperatures, and the line-of-sight (vertical) drift velocity of O^+, up to at least 1000 km height. It was found, for the period studied, that H^+ concentrations remain low even on quiet days. Whereas vertical O^+ drifts can be deduced directly from the radar data, this was not the case for H^+, since the radar is not sufficiently sensitive to the H^+ drift velocity. A method was developed and tested, in which the coupled momentum equations of the two ion species and of the electron gas are solved to deduce the field-aligned velocity of H^+ from the balance of all forces present. All terms of the momentum equations can be deduced from the observed vertical variation of radar-derived parameters, given a model of the neutral atmosphere and collision frequencies. The method used was shown to be reliable, though sensitive to the choice of O^+/O collision factor, and to give results in good agreement with present hydrodynamic models of field-aligned plasma flow. It provided a systematic estimate of O^+ and H^+ outflow fluxes at the top of the observed region, showing that H^+ velocities and fluxes are generally significantly smaller than expected for the polar wind situation. The computations for the H^+ drift velocity rely on an atmospheric model (CIRA-86) in order to compute the collision frequencies. The major neutral atomic concentrations in the model should be calibrated in order to minimize the model dependence of the calculations, ie the neutral oxygen and hydrogen concentrations for the O^+ ion energy equation and the H^+ continuity equation respectively. For the first EISCAT VHF observations used, from the July-August 1988 campaign, an overall agreement was found between the derived atomic oxygen concentration and the CIRA-86 model; for atomic hydrogen, the derived concentrations are a factor 2 to 5 greater than predicted by the model, showing a clear tendency for the model to underestimate H concentrations at high latitudes (Wu Jian, Blanc, Alcaydé, Fontanari and Kofman).

NON-MAXWELLIAN PLASMAS

For ion drift velocities larger than the thermal velocity of the neutral atmosphere, the ion velocity distribution function becomes increasingly non-Maxwellian and the shape of the incoherent scatter spectra deviates from that which is assumed for standard analysis. Model calculations have been performed to investigate this effect. As an example, Fig. 22 shows the error in the determination of T_e as a function of E_{perp}. A relaxation collision model was used for the calculations, which means that the errors are probably over-estimated, and the ratio of the collision frequency to the ion gyrofrequency was 0.6 (Cooper and Kohl).

The range of electric field amplitudes where the assumption of a bi-Maxwellian ion distribution is good enough to provide reliable measurements of electron temperature, density and ion temperature anisotropy were also determined, as functions of the ion population, and of the direction of observation relative to the magnetic field (Hubert and Lathuillère, 1989).

The effect on the errors of the assumed ion composition, in a mixture of ions O^+ and NO^+ was also studied. Because the two ion species do not have the same anisotropy, their line-of-sight temperatures will differ at all aspect angles other than 54.7°. This implies that the errors of estimation on composition and temperature are not only due to the spectral distortion, but also to the fact that the usual assumption of the same temperature for both species is no longer valid. One main conclusion is that the validity domain of the standard analysis, as a function of the parameter D^* (the ratio of the ion-neutral differential velocity and neutral

thermal velocity) and the aspect angle, is smaller for a mixture of ions than for a single ion species. Secondly, the ion composition is not well estimated, for measurements along the magnetic field line, when D* is greater than 0.5, corresponding to an electric field amplitude greater than 20 mV m^{-1} (Lathuillère and Hubert, 1989).

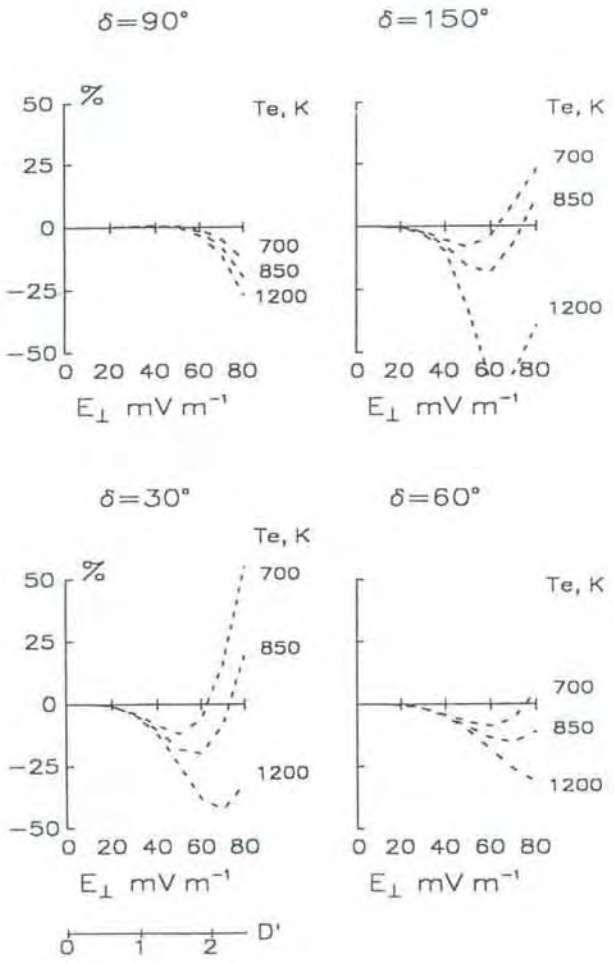

Fig. 22. Percentage departure of estimated Maxwellian electron temperature $(T_e)_{Max}$ from T_e (model) with E_{perp} and T_e (model) as parameters. The aspect angle of the radar beam relative to the magnetic field was assumed to be 54.7°. δ is the angle between the Hall direction and $\underline{k}_{perp}$ to the radar beam; δ is zero when the beam is in the plane defined by the Hall direction and $\underline{B}$.

Observations of non-thermal plasmas at different aspect angles were considered and spectra found with well-defined central peaks, consistent with ion velocity distribution functions which depart significantly from the Maxwellian form; as the aspect angle decreases, the central peak becomes less pronounced. By including mixed ion composition, a significant improvement was found in fitting some of the observed spectra. It was suggested that N_2^+ formed a significant proportion of the molecular ions during these observations. The influence of anisotropic ion velocity distributions on ionospheric ion outflows to the magnetosphere has also been studied. Such distribution functions produce an additional upward force on the F-region plasma. The magnitude of the upforce within a flow burst event was found to be fully consistent with the expected ionospheric signature of a flux transfer event. In one event, the hydrodynamic mirror force became as large as 10% of the gravitational downforce on O^+ ions at 450 km altitude (Winser et al., 1989, Lockwood et al., 1989 and Suvanto et al., 1989).

HIGH LATITUDE CONVECTION AND MAGNETOSPHERIC RESPONSES

EISCAT CP-1 electron density profiles have been compared with simultaneous solar wind parameters (B, V). It was shown that different heights in the ionosphere respond differently to solar wind changes. At high altitudes (>250 km) N_e and the solar wind parameter, V x B, were anticorrelated, probably due to enhanced recombination during disturbed conditions. At low altitudes (<100 km) the correlation between N_e and V x B was positive; this can be explained by precipitation of high energy particles triggered by solar wind changes which cause a density enhancement in the lower ionosphere. In the intermediate regime (100<h<250 km) no clear correlation was found, since the ionisation is controlled here by several processes such as chemical reactions, solar UV and convection which depend differently, or not at all, on the solar wind (Shirochkov and Schlegel).

The precipitation of magnetospheric electrons acts as a secondary source, in addition to solar illumination, of ionization and heating for ionospheric electrons. The intensity of these effects could be directly evaluated from simultaneous observations, approximately along the same magnetic field line, of precipitation fluxes at the top of the

ionosphere (by VIKING) and vertical profiles of ionospheric parameters (by EISCAT). Ionization production in active auroral forms and temperature profiles observed by EISCAT, compared to theoretical computations of the heating rate produced at each altitude by the precipitating fluxes observed by VIKING, have been considered. (Opgenoorth et al., 1989; Lilensten, Fontaine, Kofman, Lathuillère, Eliasson and Oran).

EISCAT observations in conjunction with television cameras and photometers on Spitzbergen, have revealed dramatic flow bursts in the dayside auroral oval, lasting up to 15 minutes, associated with transient auroral displays. The corresponding voltages integrated across the radar field-of-view are of the order of 60 kV and perhaps as large as 80-100 kV in total. The transient auroras form on the equatorward edge of the persistent cusp/cleft before moving into the polar cap and fading. This motion into the polar cap strongly suggests that these transients are associated with Flux Transfer Events (FTEs) at the dayside magnetopause and are not signatures of dynamic pressure pulses in the magnetosheath which should remain within or equatorward of the cleft region.

The association of transient auroras and flow bursts with FTEs has been strengthened by two separate studies. The first showed that, for continuously southwards interplanetary magnetic field (IMF), the events recurred with a mean repetition period of 8.3 +/- 0.6 min - similar to the mean repetition rate of FTEs observed at the magnetopause under the same conditions. Isolated events which occurred when the IMF was predominantly northward were consistent with each being triggered by a short-lived southward swing of the IMF. In the second study, FTEs were directly observed at the dayside magnetopause by the ISEE-2 satellite when in close conjunction with the EISCAT/optical field of view. In two cases, classic FTE signatures were followed by an optical/flow burst event in the ground-based data, Fig. 23. Flow enhancements are clearly seen in the voltages ϕ_{NS} and ϕ_{EW} (across the north-south and east-west dimensions of the radar field-of-view), similar to those previously reported, but weaker because the radar field of view did not extend as far north towards the optical arc. The dashed lines indicate a possible link between two clear FTEs, seen when ISEE-2 was in the magnetosheath, and a flow enhancement and optical arc which were observed a few minutes later. The third event may be associated with the 'BL spikes' observed by ISEE-2, a predicted FTE signature when inside the reconnection layer of the magnetopause (Lockwood et al., 1989; Elphic, Lockwood, Cowley, Sandholt, Lybekk and Farmer).

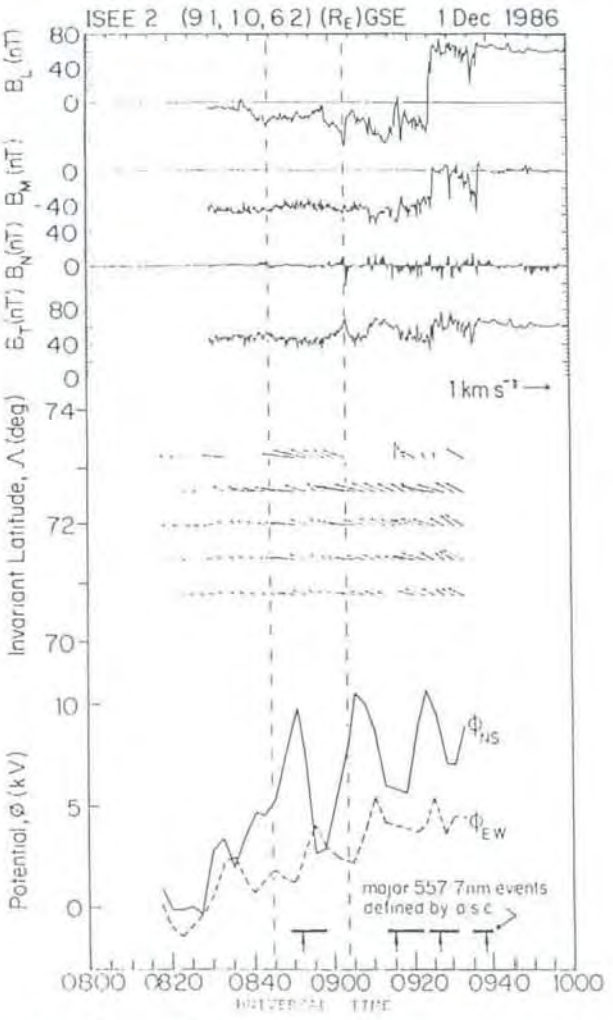

Fig. 23. ISEE observations of magnetic fields at the magnetopause, EISCAT flow data, and westward-moving 557.7 nm auroral transients observed at Ny-Ålesund, Spitzbergen.

Short-lived plasma flow-bursts have also been observed by EISCAT in the evening and midnight sector, especially during substorm activity. The most common signature is seen in the eastward electrojet when a southward burst coincides with an enhancement of the westward plasma velocity. Typically these bursts last for

about 3-7 minutes, and are repeated in a quasi-periodic sequence (Fig. 24).

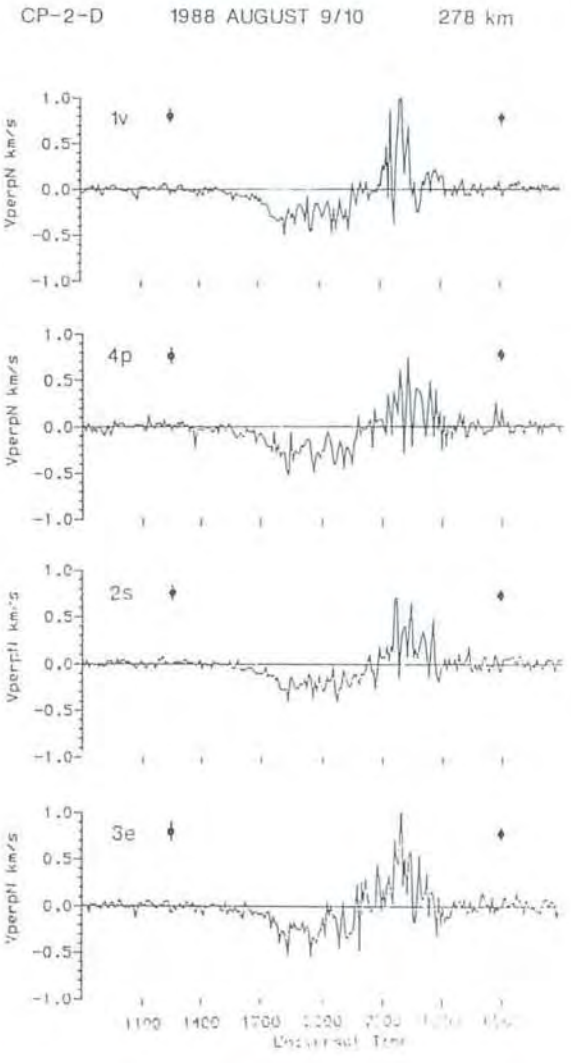

Fig. 24. Field-perpendicular plasma velocity in the north-south plane at 278 km, measured on 9-10 August 1988 for the four positions of CP-2. The errors represent typical values for the evening and midnight sectors. Equatorward bursts of plasma velocity, much larger than these errors, are seen at 1822, 1937, 2037 and 2153 UT.

To measure such rapidly varying plasma velocities it is necessary to make tristatic observations with sufficient time-resolution. Confirmation of the validity of the velocity measurements is provided by simultaneous measurements of ion temperature in the upper E and F-regions, and electron temperature in the E-region. The sudden onset of large electric fields drives the plasma at elevated velocity through the neutral atmosphere, causing substantial frictional heating at all heights above about 140 km. The same electric fields generate wave turbulence in the E-region and cause a sharp rise in electron temperature between 100 and 120 km.

EISCAT measurements alone are not able to define the total horizontal extent of such events, but on several occasions the bursts are seen in successive positions of the CP-2 cycle, showing that they are correlated over at least 130 km in the north-south direction (Fig. 24). Similar bursts are observed by the SABRE (Sweden and Britain Radar Experiment) coherent radar and these measurements confirm that the pattern can extend over several degrees of latitude and at least 10° of longitude (Williams, Virdi, Cowley and Lester).

Bursts correlated over such large areas probably represent perturbations of the whole convection pattern. For those events where simultaneous IMF measurements are available, there is strong evidence that two sources of flow are involved. A southward-turning of the IMF has a direct effect on the night-time convection pattern, with a time-lag of about 20 min, and an indirect effect, associated with rapid tail reconnection, after about an hour (Williams et al, 1989).

Dayside flow bursts have been found to show very large zonal flow velocities. On 9 February 1988 exceptionally large convection velocities attaining values of 5 km s^{-1} were observed, Fig. 25. The event lasted less than one hour, between 1530 and 1630 UT, and covered 2° between 70° and 72° geographic latitude, or about 200 km. The duration of the event implies a longitudinal extent of about 400 km. Electron and ion temperatures in this region show increased values with respect to the surroundings. The IMF was southward from 1330 UT until at least 1700 UT, and the measured ion line spectra include clear signatures of non-Maxwellian ion velocity distributions.

This event might be related to quasi-steady reconnection; however, its location and the large southward component of the flow do not fit any of the known models of reconnection. It could also be a secondary effect of an event taking place on the

antisunward part of the dusk convection cell (La Hoz and Buchert).

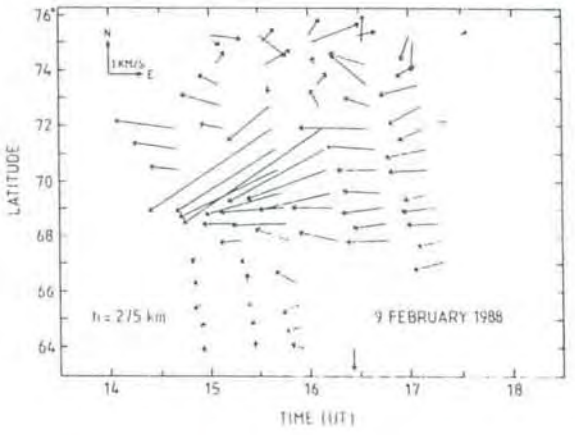

Fig. 25. Large velocities measured by EISCAT on 8 February 1988.

On 15 January 1989, even higher flow speeds appeared to peak at 6 km s^{-1}, though these measurements must be treated with caution as they were produced using a beamswinging technique. However, the ion temperatures, (estimated with allowance for non-Maxwellian distortion of the velocity distribution) had peak values of about 20,000 K, consistent with the flow speeds and a simplified form of the ion energy balance equation. At the same time, a transient depletion of the plasma densities was observed. In all range gates, the enhancement of ion temperature and the plasma depletion were observed at the western azimuth first, indicating that the event propagated eastwards over the radar field of view. The central region of eastward flow was about 250 km in north-south extent, with an associated potential of 55 kV.

In the signature of an FTE, the mean plasma flow velocity, averaged over the newly-opened flux tube, should be the same as the velocity of the event as a whole. Testing this condition is complicated by difficulties in defining the extent of the flux tube but it has been shown that the transient bursts observed by EISCAT and optical instruments can meet this criterion. For an FTE interpretation, the dimensions of the events studied are typically 100-200 km north-south and 1500-2000 km east-west. Allowing for this elongation, the flow patterns observed are consistent with FTE models. The mapping of field lines from magnetopause to ionosphere is uncertain, but the large zonal dimensions of such events support recent theories of FTEs in terms of time-dependent reconnection at an elongated X-line (Lockwood, Cowley, Sandholt and Lepping).

The dayside cleft aurora is thought to map to the low-latitude boundary layer (LLBL) of the magnetosphere. POLA observations, in conjunction with optical observations on Spitzbergen, have revealed flow signatures around patches of auroral luminosity at 14 MLT, seemingly in the cleft region. Fig. 26 shows flow vectors derived by EISCAT, superimposed on the one-second images of such a patch, observed by a 630 nm CCD all-sky camera at Ny-Ålesund. As the patch drifts eastward (tailward), enhanced flows are observed which are initially westward and then swing eastward. Although errors are introduced by the assumptions inherent in the beamswinging technique the observed enhancements of ion temperature are generally consistent with the derived flows.

Fig. 28 shows a similar event near magnetic noon. Again the derived flows contain errors, particularly at the highest latitudes where the beam separation is very large, but the velocity of the 557.7 nm auroral forms, deduced from the all-sky TV camera, is very close to the local plasma flow, as measured by EISCAT. Further justification comes from the ion temperatures estimated from the ion flow vectors; with a number of simplifying assumptions, these compare well with the temperatures actually observed by the radar. Important differences can be found, but the ion temperatures verify the major features of the event as deduced from the beamswinging technique. The patches of 630 nm aurora are thought to be related to blobs of enhanced magnetosheath-like plasma which have been observed in the low-latitude boundary layer (LLBL); the flow signatures may help adjudicate between several theories for populating the LLBL. (Sandholt, Lockwood, Lybekk and Farmer; Lockwood, Sandholt, Farmer, Cowley, Lybekk and Davda)

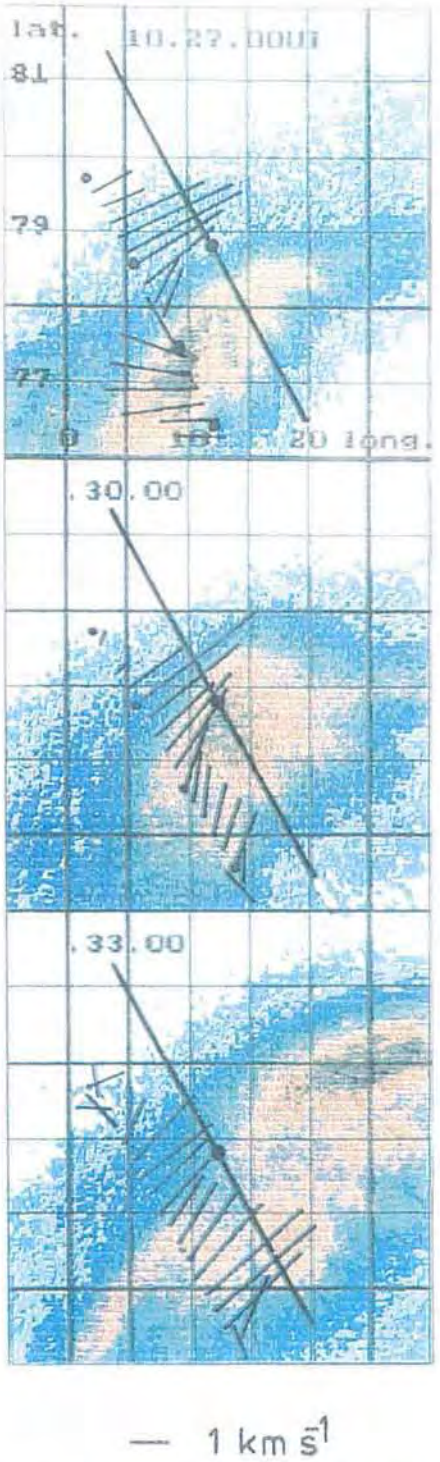

Fig. 26. Sequence of 1-second images from the 630 nm CCD all-sky camera at Ny-Ålesund, Spitzbergen. An easterly patch of 630 nm luminosity can be seen at 14 MLT. Simultaneous flow vectors from EISCAT are also shown. The solid line indicates the magnetic meridian at Ny-Ålesund. The colour scale shows relative intensity with white as the weakest and blue as the strongest emission. (Sandholt, Lockwood, Lybekk and Farmer).

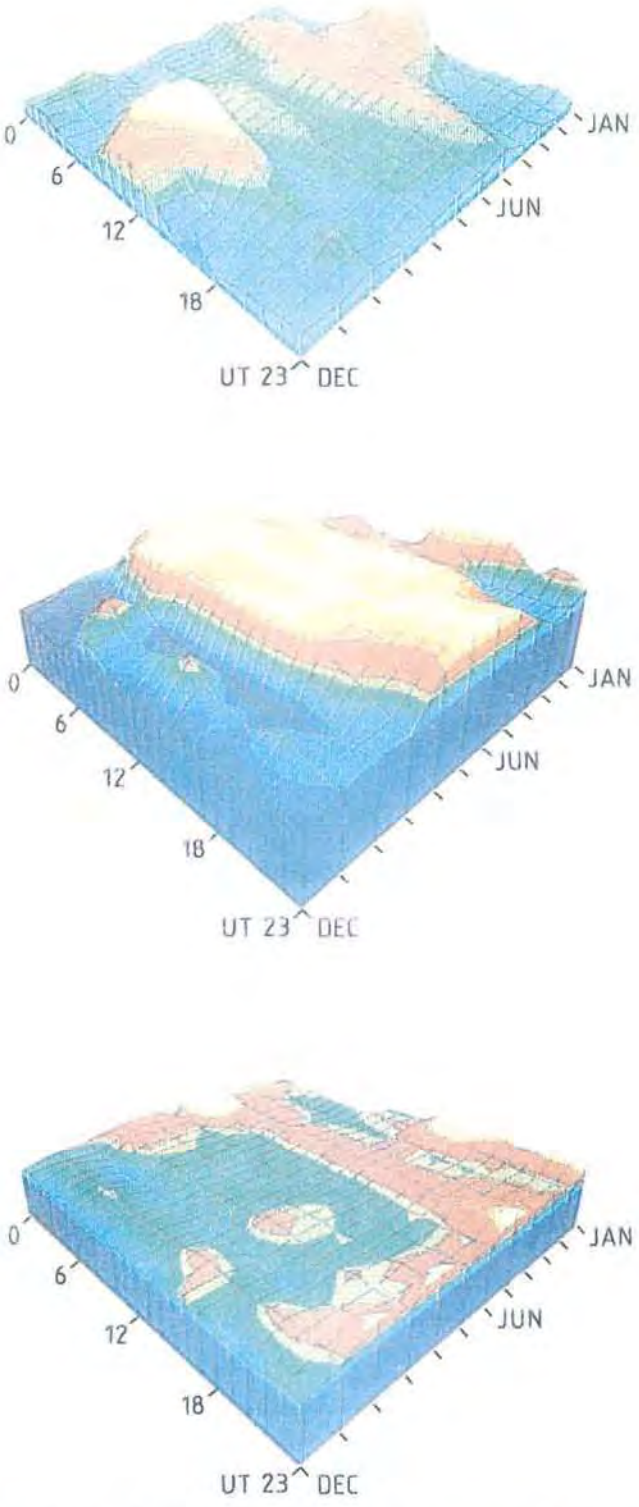

Fig. 27. Average ionospheric parameters from EISCAT Common Programme data observed along the Tromsø field line over the height range 300-350 km at sunspot maximum (January 1988 - August 1989). The average electron concentration, N_e, electron temperature, T_e, and ion temperature, T_i, are shown as functions of UT and month. The colour scales run from blue to yellow and correspond to a range of 900-1600 K for T_i (lower panel), 1400-2600 K for T_e (middle) and 0-1000 10^9 m^{-3} for N_e (upper panel). (Farmer, Fuller-Rowell and Quegan)

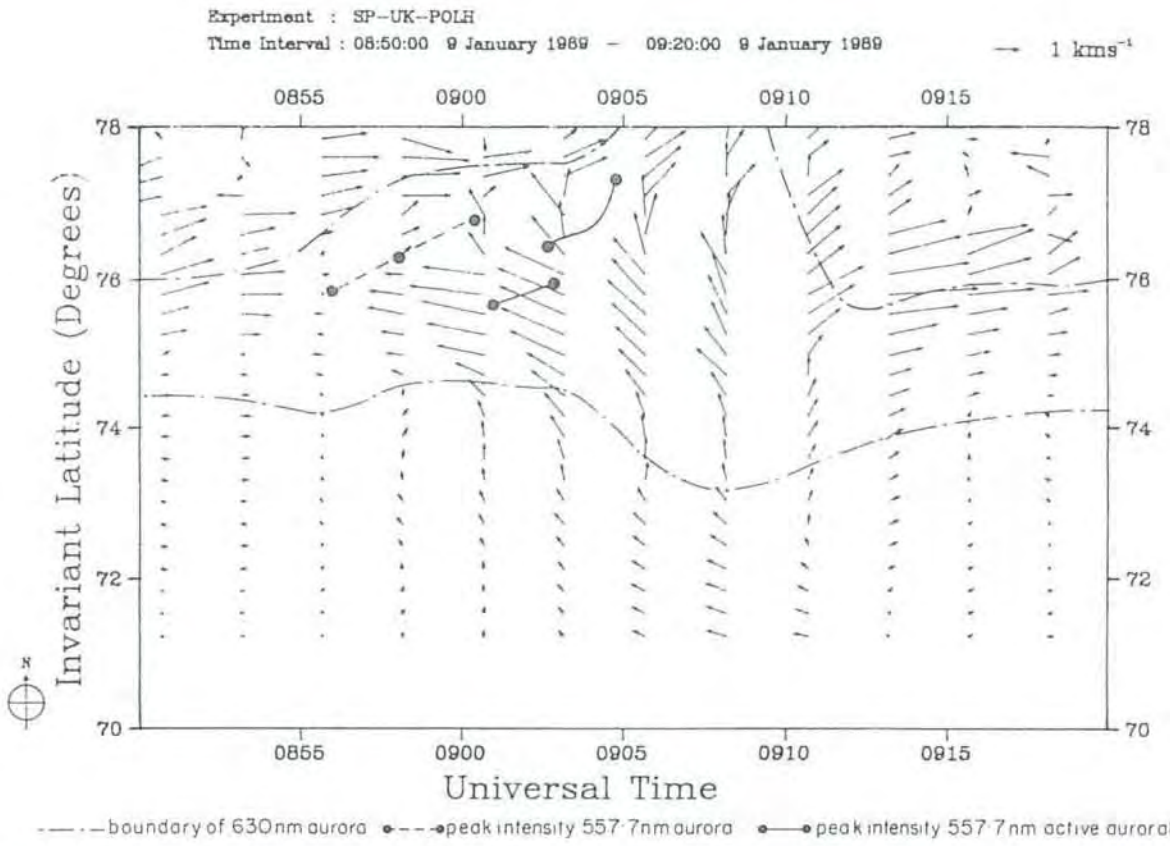

Fig. 28. Transient flow/auroral event observed near noon by EISCAT and optical instruments at Ny-Ålesund, Spitzbergen. The observed broadening and intensification of the band of 630 nm aurora and the transient active 557.7 nm auroral forms in the cusp/cleft region are accompanied by transient swings to westward and then eastward plasma flow (Lockwood, Cowley, Sandholt and Lepping).

The response of the evening sector auroral oval ionosphere to a geomagnetic sudden commencement has been studied with the CP-1 data. Immediately following the magnetic impulse, EISCAT observed a similar impulse in the poleward electric field and in the F-region ion temperature (Fig. 29). During the hour following the impulse, a strong depletion of the, still sun-lit, F-region developed, along with further increases in electric field and ion temperature. Ionosondes further south detected the equatorward progression of the depletion. These observations were consistent with an equatorward expansion of the high latitude convection pattern following the magnetic impulse, the depleted densities being brought into the radar field of view by westward convection of low density nightside plasma (Collis and Häggström).

More quantitative investigation of the increases of ion temperature at 279 km altitude, and of the electric field, during the development of the density depletion showed that the derived ion temperature did not increase as much as would be expected if the ion-neutral energy balance were maintained. It was suggested that the low ion temperatures were an artefact of the assumption of a wrong model for ion composition in the data analysis.

A second analysis, in which the ion temperatures were fixed to the values expected from energy balance considerations, allowed the changes in ion composition to be determined during the depletion. Significant increases in electron temperature were predicted by the second analysis and a depletion of O^+ content to only 10% was observed in one example, Fig. 30 (Häggström and Collis).

The effects of magnetospheric convection on the high-latitude atmosphere have been included in the University College-Sheffield three-dimensional, coupled ionosphere-

thermosphere model, and the predictions of this model have been compared with averaged ionospheric parameters from EISCAT's Common Programmes (Fig. 27). Initial comparisons for medium to high levels of solar activity showed good agreement, with the numerical model closely reproducing the diurnal variations of the real data in winter and summer (Farmer, Fuller-Rowell and Quegan).

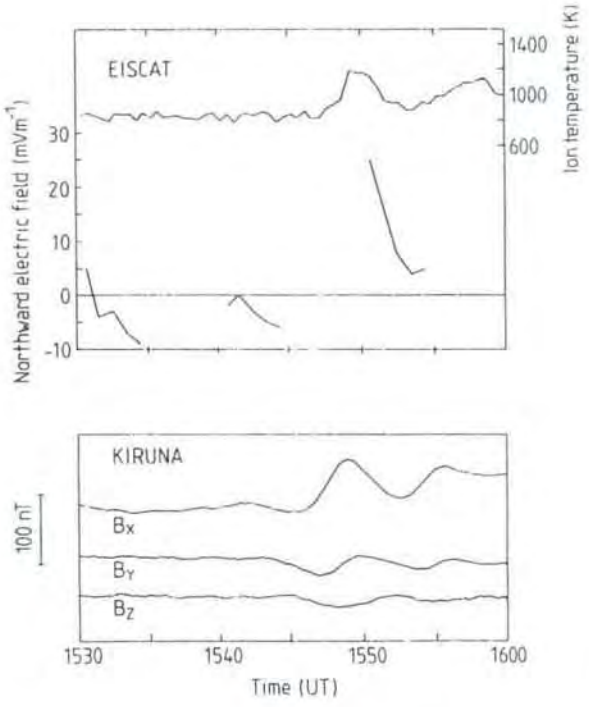

Fig. 29. Detailed comparison of T_i, electric field (both measured by EISCAT at 279 km) and magnetic field variations at Kiruna on 25 March 1987. Gaps in the E field measurements are a result of the scanning programme.

Auroral convection has been studied using simultaneously the Millstone Hill, EISCAT and Søndrestrøm incoherent scatter radars. A series of convection 'snapshots' made during an interval of increasing geomagnetic activity indicate that the large-scale convection pattern maintains a two-cell character during substorm onset and that average models derived from radar data provide a reasonable representation of the large-scale convection pattern during dynamically varying conditions. A substorm observed by the Søndrestrøm radar, and auroral and midlatitude magnetometers, was associated with a polar cap contraction observed near dusk by EISCAT and substorm flow surges, observed near midnight by Søndrestrøm, were associated with rapid contraction of the polar cap near dawn, as observed by EISCAT. Further studies have been made with Søndrestrøm either at dawn or noon while EISCAT was observing in the noon and afternoon sectors respectively. Observations during southward turnings of the IMF (observed by the IMP-8 satellite) show that the onset of enhanced convection occurred first at the radar closest to noon, as predicted for the model of ionospheric convection derived from the EISCAT-AMPTE data on ionospheric response times (Foster et al., 1989; Clauer et al 1989; Lockwood et al., 1989; Lockwood and Freeman, 1989; Robinson, R., Clauer, de la Beaujardière, Kelly, Friis-Christensen and Lockwood; Lockwood).

Electric fields and conductivities derived from EISCAT data during the two GISMOS campaigns of January 1984 and September 1986 were included in the NCAR data base and combined with observations from other incoherent scatter radars, from HF radars, from ground-based magnetometers and from satellites, to map the instantaneous large-scale electric potential pattern in the auroral and polar regions, using the AMIE technique described by Richmond and Kamide (1988).

During periods of high magnetic activity, convection electric fields can penetrate directly towards middle and low latitudes. The electrical coupling between the high, middle and low-latitude ionospheres was examined using data from five incoherent scatter radars including EISCAT, together with interplanetary and ground-based magnetic data, for the GISMOS period in January 1984. This data set shows that the theoretical global convection models reproduce roughly the main characteristics of the middle and low latitude electric fields associated with the variations of the cross-polar-cap potential drop. However, substantial disagreements between observations and models may appear, and could be due to the action of the disturbance dynamo effects on middle and low latitude electric fields (Fejer, Kelley, Senior, de la Beaujardière, Holt, Tepley, Burnside, Abdu, Sobral, Woodman, Kamide and Lepping).

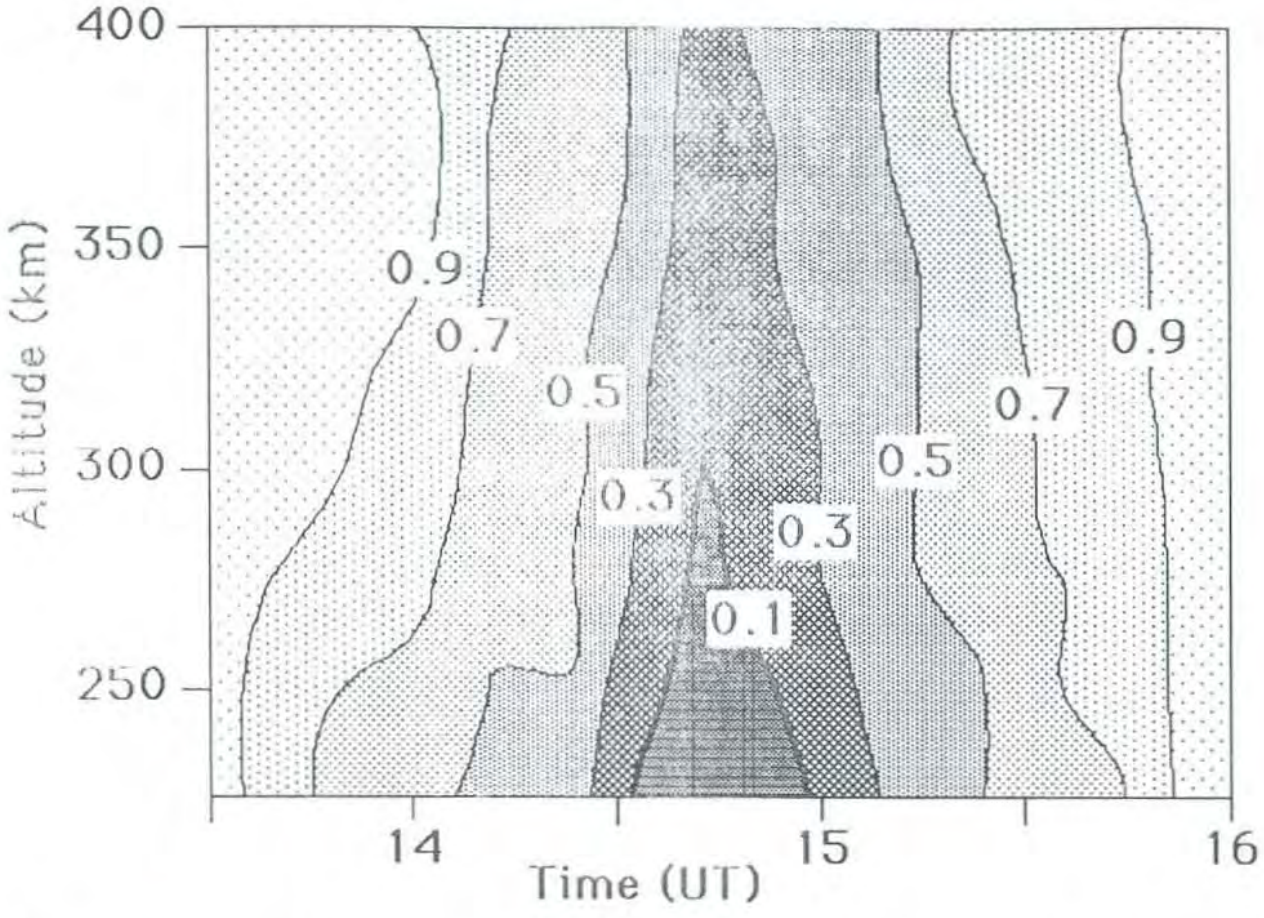

Fig. 30. Contours of O^+/N_e between 225 and 400 km on 28 July 1987 as derived from the composition-dependent analysis.

EISCAT tristatic ion velocities from CP-3 data obtained between June 1984 and November 1987 were used to construct empirical statistical models of convection electric fields and electrostatic potential as a function of Kp. These models provide estimates of the total potential drop in the field of view of the radar (a lower estimate of the total cross-polar-cap potential) and of its variation with Kp. They also show how the latitudinal and longitudinal extensions of the convection cells, the rotation of the potential pattern relative to the noon-midnight meridian and the penetration of the electric fields towards mid-latitudes vary with geomagnetic activity. The comparison between these models and those obtained from the Millstone Hill and Chatanika radar data shows generally good agreement, with slight differences due to the geographic locations of the three radars (Senior, Fontaine, Caudal, Alcaydé, Fontanari).

In a multi-radar study of the main F-region trough during the SUNDIAL interval in September 1986, the trough was tracked from EISCAT, to Søndrestrøm and Millstone Hill. The observations of the trough at EISCAT and Søndrestrøm were predominantly in the noon and post-noon local time sectors, when the trough is associated with strong westward convection. At Millstone Hill this was also the case in the pre midnight sector, but in the post-midnight sector the trough occurred equatorward of the region of largest eastward flow. These observations suggest that the trough may have different generation mechanisms at different local times, or that, once formed in the post-noon sector, the trough tends to co-rotate as a structure within the ionosphere (Foster, Foster, Wickwar and Gustafsson).

Large scale plasma structures, manifesting as local electron density enhancements which travel over large distances in the high latitude and polar cap ionosphere, so called 'blobs', have been studied with EISCAT. Not only electron density, but also ion and electron temperatures inside the blobs, have been studied simultaneously for the first

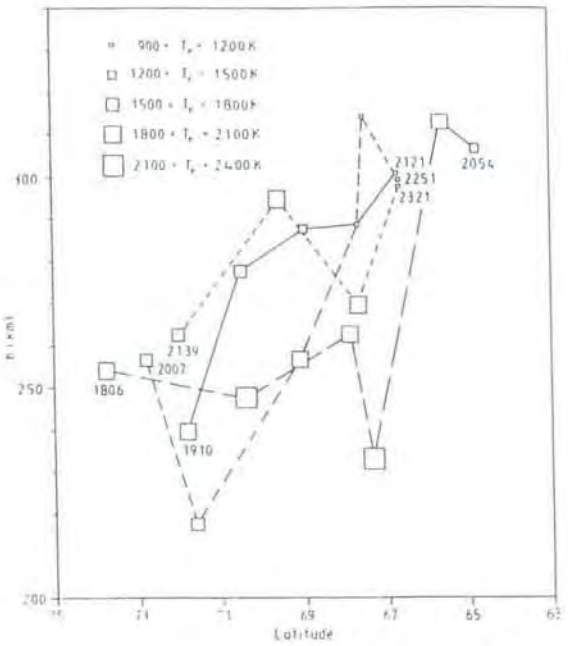

Fig. 31. Life history of 'blobs' obtained from consecutive EISCAT CP-3 scans

time. While the ion temperatures show no peculiarities, the electron temperature is quite variable. A positive correlation of T_e with blob geographic latitude, and a negative correlation with blob altitude, were found. From consecutive CP-3 scans, 'life-histories' of blobs were derived (Fig. 31); they originate at high latitudes and low altitudes, probably due to particle precipitation, (lower left corner, Fig. 31) and propagate towards lower latitudes and greater altitudes (upper right, Fig. 31). The electron temperature in the blob tends to decrease with time, being clearly enhanced after the blob is created and falling as it travels through the ionosphere (Chen and Schlegel).

In thirty CP-3 experiments, between 1982 and 1987, similar characteristics of the electron density and ion temperature (in the altitude range 250 to 350 km), as functions of magnetic local time and invariant magnetic latitude during 24 hours of observation, can be found in twelve cases. The most important of these is a large early morning depression of N_e, with an increase in T_i at the same MLT and invariant latitude. The electron density profile, and its variation with time, depends on the production of ion-electron pairs due to solar radiation, the recombination of the ions and their transport due to diffusion, neutral drag and the electric field. Often the electric field is greater than 10 to 20 mV m^{-1}, inducing an anisotropy of the pressure gradient and increasing the rate of O^+ recombination. All these physical phenomenon were included in a software code which simulates the electron density as a function of time in three dimensions. The calculations show that the depression is due mainly to a recombination process caused by an increase of the electric field and consequently to an increase of the effective temperature for O^+ loss (Taieb, 1989).

OTHER SCATTERING PHENOMENA

Gyro Line Observations

Electron gyro line observations were made with the EISCAT UHF radar in the summer of 1989. The gyro line echo is displaced by a frequency $f = (2\pi)^{-1} \Omega \cos(\theta)$ from the normal ion line spectrum (where Ω is the electron gyro frequency and θ is the angle between the directions of the wave vector and the magnetic field). At UHF the line is usually very broad and difficult to detect, but numerical simulations show that it might be observable at altitudes of 100-120 km, where both the Landau and the collisional damping are not critical. An experiment was therefore performed to investigate this possibility, where the UHF antenna was pointed 45° east of north at an elevation of 10°. This gives θ between 83.5° and 82.5° for backscatter at 100-120 km. Strong echoes were received from about 100 km altitude. Fig. 32 is an example of the returned power in a 12.5 kHz wide band upshifted by 150 kHz with respect to the transmitter frequency. Echoes were only seen in this band or the neighbouring band at 125 kHz (the calculated gyro line offset is 138 kHz). Ten examples of such signals were found altogether but none lasted for more than 30 s. At the time, the geomagnetic field was very disturbed and there was a very high proton flux (PCA) accompanied by strong X-ray radiation. These conditions must be responsible in some way for the strong excitation mechanism necessary to overcome the damping and explain how the gyro line can be excited to such a high level.

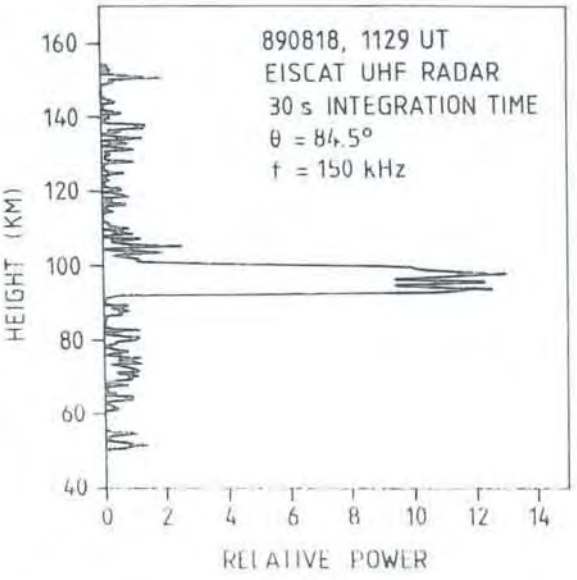

Fig. 32. Gyro line return measured on 18 August 1989, with the EISCAT UHF radar pointing 45° east of north at an elevation angle of 10°. θ is the aspect angle and f is the offset frequency of the receiver filter.

Coherent E-region echoes observed at UHF

Coherent echoes in the auroral E-region, from plasma instability produced irregularities, have been further investigated, particularly their fine structure in space and time.

High resolution measurements showed that the echo structures are highly variable. The altitude of the strongest backscatter is usually less than 110 km but the measured width of the structures, 6 km, is probably a function of the antenna beam width; the true thickness of the layers being somewhat smaller. Often an apparent downward motion of such structures is observed but this is more likely to be motion in range, since the observations are made at low elevation. The occurrence of single 'blobs' in a contour plot of height/range versus time are interpreted as structures convecting through the antenna beam (Fig. 33).

High time resolution was obtained using a special correlator program which recorded the individual return of each radar pulse. The distribution of the backscatter amplitudes was found to be approximately a Rice distribution, with a Rice parameter a = 3.7, indicating reflections from ordered structures in the scattering volume (Bragg-condition) together with noise. The shape of the backscatter spectrum did not change when the integration time was reduced from 5 s to 100 ms (Schlegel, T. Turunen and Moorcroft).

COHERENT AND INCOHERENT SCATTER RADAR COMPARISONS

The distorted ion velocity distribution associated with large ion drifts in the auroral F-region drive ion-cyclotron waves - the ion cyclotron micro-instability. By taking into account the Landau damping of these waves, by electrons, it has been shown that the instability can be exited for all values of T^*/T_e, where T^* is the field parallel ion temperature and T_e the electron temperature. The existence of microstructure in the distribution of electron concentration within a scattering volume can cause non-linear effects in the relationship between the irregularity drift velocity measured by coherent radars and the electron drift velocity measured by an incoherent scatter radar. A study has shown that, for large electric fields, the strongest scattered signals come from regions where the electron concentration is above average and the

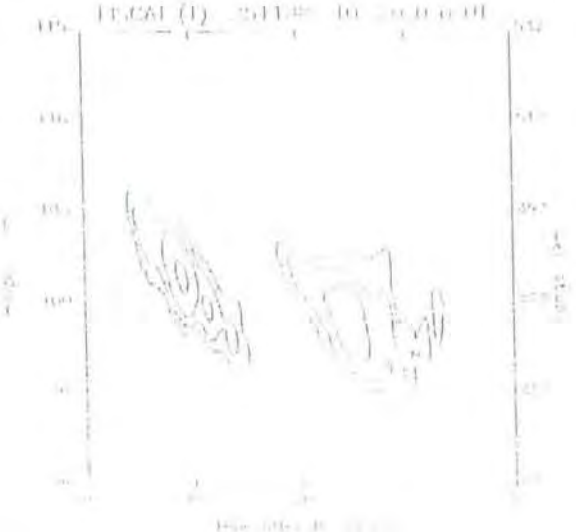

Fig. 33. Structures in range/height and time of coherent backscatter produced by E-region plasma instabilities.

electric field below average, leading to an underestimate in the drift velocity measured by the coherent radars (Suvanto, 1989; Uspensky et al., 1989).

A theoretical study of UHF coherent backscatter has also been undertaken in support of the new Coherent Scatter (COSCAT) experiment. The calculations predict that coherent echoes received by the EISCAT UHF receivers from the remote COSCAT transmitter should have phase speeds significantly higher (20-30%) than those detected by VHF radars such as STARE and SABRE. The first COSCAT measurements have now been made and preliminary analysis of the data indicates that the coherent spectra received are very similar to the type 1 spectra received at VHF (T. Robinson and Honary).

IONOSPHERIC MODIFICATION (HEATING)

EISCAT observations during high-powered radio-wave modification of the ionosphere at Tromsø indicate large increases in T_e associated with the Heater turn-on. Detailed analysis of these data has revealed exciting new evidence for a heater-induced thermal cavitation effect. The temperature data typically indicated a peak in $\Delta T_e/T_e$ (the relative change in electron temperature) of 40% in the vicinity of the heater reflection height, which was usually close to 200 km. Above the peak, $\Delta T_e/T_e$ falls off approximately exponentially as the altitude increases, with a scale length of a few ten kilometres. Below the peak, $\Delta T_e/T_e$ falls off more quickly. The EISCAT observations also indicated that the temperature changes saturate after about two minutes of heating. The change in electron concentration, $\Delta N_e/N_e$, typically reaches a maximum of 30% at a height close to the initial interaction height and falls to zero 20 km higher. Below the maximum, $\Delta N_e/N_e$ falls to 5% and then rises to a second maximum, of about 20%, 20 km below the initial heater interaction height. The trough in $\Delta N_e/N_e$ constitutes strong evidence for heater-induced cavitation (Robinson, 1989).

In an ionospheric HF-modification experiment for which the Heater was operated at 4.04 MHz and modulated 20 s on, 40 s off, EISCAT observed waves propagating parallel to B_o, and chirped, as well as normal, plasma line observations were performed. Heater-induced plasma lines were observed only in the first 10 s integration interval, indicating a strong overshoot.

These lines are unusual in that multiple simultaneous lines were observed, normally originating within one kilometre of the critical region but sometimes from lower heights, and that the frequency of the most constant line is offset some 250 kHz from the heating frequency, with the other lines occurring at greater frequency offsets. The natural, photo-electron enhanced, plasma line was not observed; however, the background plasma parameters were measured using ion line observations. Comparisons with chirped observations, performed at EISCAT in May 1986, indicate that increased Landau damping may be responsible for both the strong induced-line overshoot and the lack of a distinct natural line. Ion line power profile observations show the existence of a topside enhanced ion line at the critical density corresponding to the heater frequency. It is believed this is due to strong O/Z-mode coupling parallel to B_o and low values of foF2. These phenomena are illustrated in Figs. 34 and 35 (Isham, Kofman, Hagfors, Nordling, Thide, La Hoz, Stubbe).

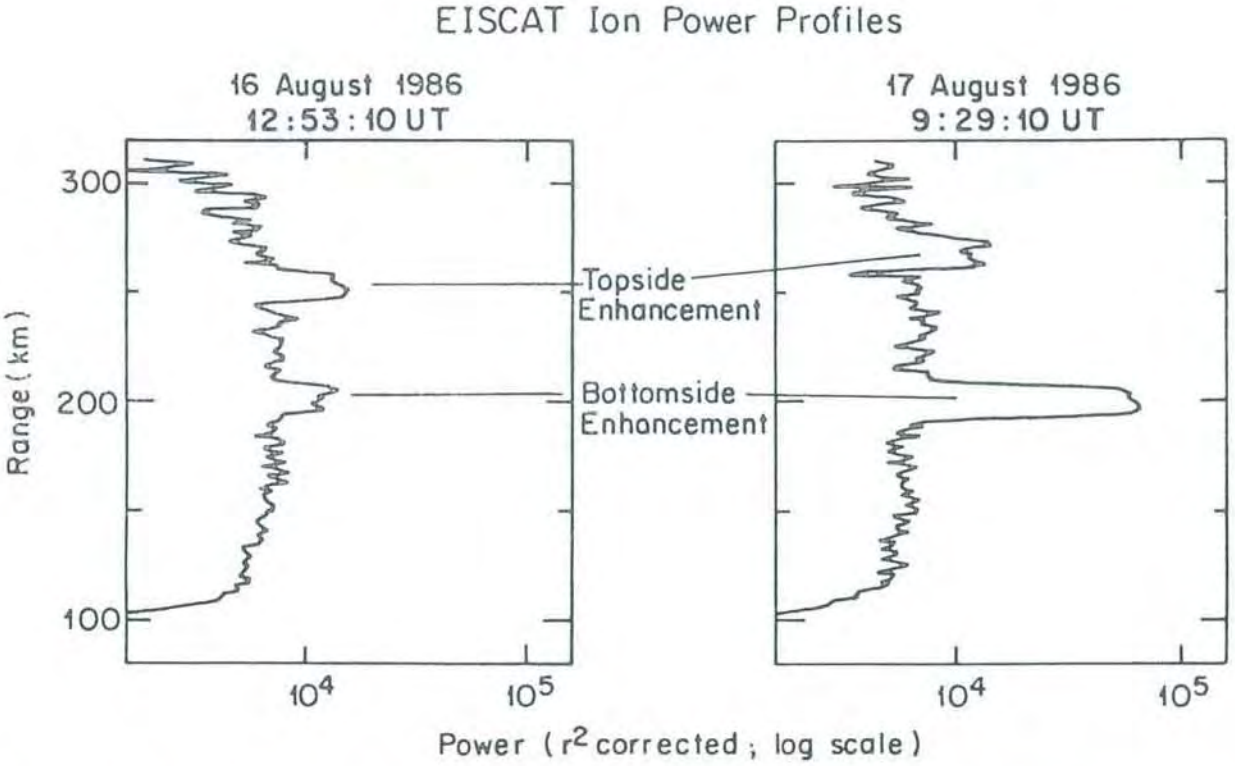

Fig. 34. Power profiles of the incoherent scatter ion line measured during ionospheric modification experiments at EISCAT. There is clear evidence of enhancement both at the lower reflection level: $x = (\omega_p/\omega) = 1$, and in the topside F-region, where x is also unity.

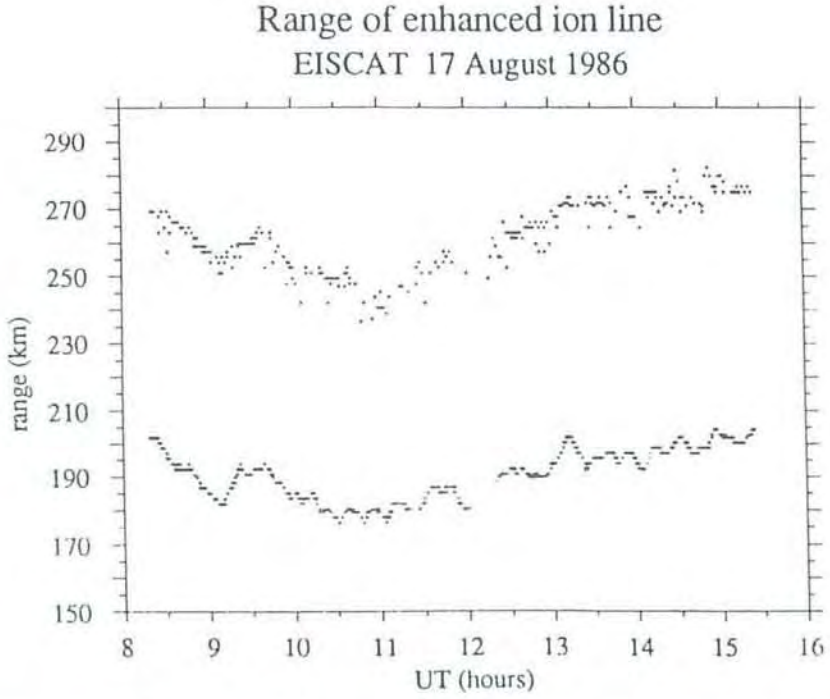

Fig. 35. The heights of the lower and upper ion line power enhancement plotted as a function of time for the observations of 17 August 1986.

NEW DIGITAL SIGNAL PROCESSING DEVELOPMENTS

It was stressed in the minutes of the autumn 1988 Science Advisory Committee (SAC) meeting, that advances in coding and signal processing are among the most cost-effective ways to get more and better science out of the EISCAT operation, and that new developments in these areas should be given high priority. In keeping with that policy, this year's technology report concentrates on two Digital Signal Processing (DSP) development projects: the hardware decoder for alternating codes and the digital FFT processor.

Experiments based on alternating codes have already become commonplace at EISCAT, but the limited result memory of the correlator has made it almost impossible to use 32 baud codes and experiments using 16 baud codes have been forced to sacrifice time resolution in order to achieve a practical number of gates. Also, decoding alternating code modulations in the correlator has been impossible because of the lack of a programmable add/subtract function in the accumulator. However, the throughput rate of the correlators is sufficiently high to make it attractive to search for a practical way of adding this feature.

A detailed study of the correlator architecture showed that it would be relatively simple to add a hardware device to the multiplier input structure, which could manipulate the sign of an individual sample being used as one factor in a partial product. There were also some 'spare' bits in the microprogram word, which had been assigned to features which are never used in normal operation, and these could be re-assigned to the control of the added hardware. A decoder unit based on this concept has now been designed and constructed (Fig. 36). At the end of the year, is was undergoing tests in the Kiruna site correlator.

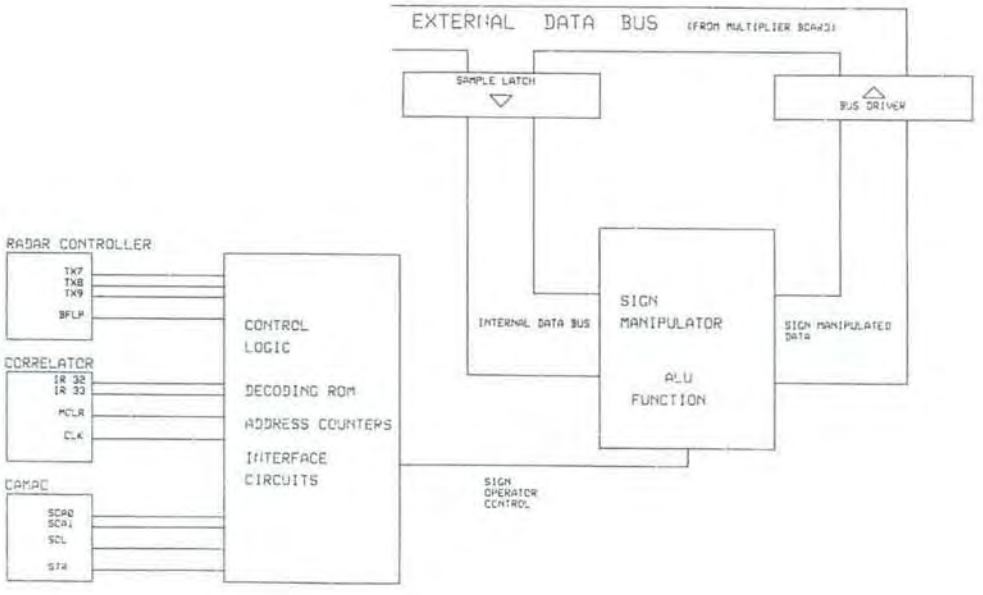

Fig. 36. Block diagram of the EISCAT alternating code decoder.

Within the new device, tables of the sign sequences for the only 32 baud alternating code known (at present) and some of the possible sixteen and eight bit codes are stored in PROM (programmable read only memory). One sample at a time is fetched from the buffer memory and stored in a register where its sign can be manipulated according to a control signal which is the binary exclusive OR of two sign sequences read from the PROM tables. The 're-signed' sample is then multiplied with another sample fetched from the buffer memory and the product accumulated to the result memory. When computed in this way, all partial sums at a certain lag become properly decoded and can be summed on top of each other in the result memory, resulting in a range-gated output whose range extent is no longer restricted by the amount of memory available.

The practical limitation of this decoding scheme is the time needed for computing the large number of cross products, many of which are actually recomputed with different sign sequences for each range gate to which they contribute. Nevertheless, very practical range coverage can be achieved before the computation time begins to limit the experiment performance. As an example, a 32 baud code requires a computation time of 112 μs per range gate. In a dedicated E-region experiment, this code can be handled for some 30 gates without having to sacrifice more than some 2% of the possible duty cycle. For a baud length of 10 μs, this corresponds to a range coverage of about 45 km (eg 90 - 135 km), which encompasses the main region of high conductivity. Shorter codes, or coarser spatial resolution, can be used to extend the range coverage.

The decoding devices are small - they occupy only two, single height, Eurocards which can be fitted in unused space towards the rear of the correlators - and they can be programmed through the correlator microprogram words for any code length. Truncated code sets are also tolerated through proper programming, and any mixture of coded and non-coded modulations can be handled. For extremely poor signal-to-noise (S/N) ratios, the nett gain in the rate of statistics is on the average two to four times compared to that of the present CP-1/CP-2. When the decoders have been installed at all three sites, alternating code modulations can be used not only for the E-region but also for velocity estimation from a measurement at collisionless altitudes, resulting in even more effective experiments. It is likely that the Scientific Advisory Committee (SAC) will be recommended to approve modified Common Programmes employing alternating code schemes as soon as the hardware and software have been validated.

The alternating code decoder is a typical in-house product. However, the new fully digital FFT (fast Fourier transform) processor is the result of an unprecedented collaboration between EISCAT, the Swedish Institute of Space Physics and the FFT chip manufacturer. The processor is a one board design using a commercial chip-set to achieve performance between ten and twenty times better than the existing CCD spectrum analyser. It was originally designed at the Kiruna site in 1988, but has now been fully integrated by an EISCAT engineer during a two month visit to the semi-conductor manufacturer's plant, where he enjoyed access to proprietary development tools and evaluation software.

The prototype FFT processor occupies a dual Eurocard and conforms to the VME bus standard. It can perform a 512 point complex FFT in just 104 μs, which makes it a very powerful tool for plasma line studies and ionospheric modification diagnostics.

PUBLICATIONS

Publications (Journals, Books), 1989

Araki, T., K. Schlegel and H. Lühr, Geomagnetic effects of the Hall and Pedersen current flowing in the auroral ionosphere, J. Geophys. Res., 94, 185-199, 1989.

Bjørnå, N., Derivation of ion-neutral collision frequencies from a combined ion line/plasma line incoherent scatter experiment, J. Geophys. Res., 94, 3799-3804, 1989.

Brekke, A., C.M. Hall and T.L. Hansen, Auroral ionospheric conductances during disturbed conditions, Ann. Geophys., 7, 269-280, 1989.

Brekke, A., C.M. Hall and T.L. Hansen, EISCAT studies of the auroral ionosphere conductances, Adv. Space Res., 9, 35-38, 1989.

Clauer, C.R., J.D. Kelly, M. Lockwood, R.M. Robinson, J.M. Ruohoniemi, O. de la Beaujardière and L. Hakkinen, June 1987 GISMOS experiment: preliminary report on high time-resolution, multi-radar measurements, Adv. Space Res., 9, 29-33, 1989.

Collis, P.N. and I. Häggström, High resolution measurements of the main ionospheric trough using EISCAT, Adv. Space Res., 9, 45-48, 1989.

Etemadi, A., S.W.H. Cowley and M. Lockwood, The effect of rapid changes in ionospheric flow on velocity vectors deduced from radar beam-swinging experiments, J. atmos. terr. Phys., 51, 125-138, 1989.

Foster, J.C., T. Turunen, P. Pollari, H. Kohl and V.B. Wickwar, Multiradar mapping of auroral convection, Adv. Space Res., 9, 19-27, 1989.

Fredriksen, Å., N. Bjørnå and T.L. Hansen, First EISCAT two-radar plasma-line experiment, J. Geophys. Res., 94, 2727-2732, 1989.

Hall, C.M., Recent D-region research using incoherent scatter radar, Adv. Space Res., 9, 163-172, 1989.

Hubert, D. and C. Lathuillère, Incoherent scattering of radar waves in the auroral ionosphere in the presence of high electric field and measurement problems with EISCAT facilities, J. Geophys. Res., 94, 3653-3662, 1989.

Huuskonen, A., High resolution observations of the collision frequency and temperatures with the EISCAT UHF radar, Planet. Space Sci., 37, 211-221, 1989.

Kaila, K. and R. Rasinkangas, Co-ordinated photometer and incoherent scatter radar measurements of pulsating arcs with high time resolution, Planet. Space Sci., 37, 545-553, 1989.

Kaila, K., R. Rasinkangas, P. Pollari, R. Kuula, J. Kangas, T. Turunen and T. Bösinger, High-resolution measurements of pulsating aurora by EISCAT, optical instruments and pulsation magnetometers, Adv. Space Res., 9, 53-56, 1989.

Kersley, L., C.D. Russell and S.E. Pryse, Scintillations and EISCAT investigations of gradient-drift irregularities in the high-latitude ionosphere, J. atmos. terr. Phys., 51, 241-247, 1989.

Kirkwood, S. and P.N. Collis, Gravity wave generation of simultaneous auroral sporadic E-layers and sudden neutral sodium layers, J. atmos. terr. Phys., 51, 259-269, 1989.

Kirkwood, S., L. Eliasson, H.J. Opgenoorth and A. Pellinen-Wannberg, A study of auroral electron acceleration using the EISCAT radar and the Viking satellite, Adv. Space Res., 9, 49-52, 1989.

Knipp D.J., A.D. Richmond, G. Crowley, O. de la Beaujardière, E. Friis-Christensen, D.S. Evans, J.C. Foster, I.W. McCrea, F.J. Rich and J.A. Waldock, Electrodynamic patterns for September 19, 1984, J. Geophys. Res. 94, 16913-16924, 1989.

Kofman, W., The F and E-region studies by incoherent scatter radar, Adv. Space Res., 9, 7-17, 1989.

Kofman, W., K. Schlegel, U.P. Løvhaug, M. Lockwood and K.J. Winser, Comment on 'The effect of strong velocity shears on incoherent scatter spectra: a new interpretation of unusual high-latitude spectra', Geophys. Res. Lett., 16, 337-338, 1989.

Kustov, A., M. Uspensky, A. Huuskonen, J. Kangas and E. Nielsen, On the threshold electric field for 1 m irregularity appearance, J. Geophys. Res., 94, 12043-12048, 1989.

Lanchester, B.S., H. Rishbeth, T. Nygrén, L. Jalonen and T. Turunen, Wave activity, F1-layer disturbance and a sporadic E layer over EISCAT, J. atmos. terr. Phys., 51, 179-196, 1989.

Lathuillère, C. and D. Hubert, Ion composition and ion temperature anisotropy in periods of high electric fields from incoherent scatter observations, Ann. Geophys., 7, 285-296, 1989.

Lehtinen, M., On optimization of incoherent scatter measurements, Adv. Space Res., 9, 133-141, 1989.

Lockwood, M., S.W.H. Cowley, C.R. Clauer, H. Todd, S.R. Crothers and D.M. Willis, Ion flows and heating at a contracting polar-cap boundary: GISMOS observations indicating viscous-like interaction on the flanks of the magnetotail, Adv. Space Res., 9, 39-44, 1989.

Lockwood, M. and M.P. Freeman, Recent ionospheric observations relating to solar wind-magnetosphere coupling, Phil. Trans. Roy. Soc., A, 328, 93-105, 1989.

Lockwood, M., P.E. Sandholt and S.W.H. Cowley, Dayside auroral activity and momentum transfer from the solar wind, Geophys. Res. Lett., 16, 33-36, 1989.

Lockwood, M., P.E. Sandholt, S.W.H. Cowley and T. Oguti, Interplanetary magnetic field control of dayside auroral activity and the transfer of momentum across the dayside magnetopause, Planet. Space Sci., 37, 1347-1366, 1989.

Lockwood, M., K. Suvanto, K.J. Winser, S.W.H. Cowley and D.M. Willis, Incoherent scatter radar observations of non-Maxwellian ion velocity distributions in the auroral F-region, Adv. Space Res., 9, 113-118, 1989.

Moffett, R.J., G.J. Bailey, S. Quegan, Y. Rippeth, A.M. Samson and R. Sellek, Modelling the ionospheric and plasmaspheric plasmas, Phil. Trans. R. Soc. Lond., A, 328, 255-270, 1989.

Natorf, L., A.W. Wernik, E.G. Wodnicka and K. Schlegel, Detecting travelling ionospheric disturbances in incoherent scatter data using the Maximum Entropy Method, J. atmos. terr. Phys., 51, 389-400, 1989.

Nygrén, T., Studies of sporadic E-layer using the EISCAT incoherent scatter radar, Adv. Space Res., 9, 73-81, 1989.

Nygrén, T., B.S. Lanchester, L. Jalonen and A. Huuskonen, A method for determining ion-neutral collision frequency using radar measurements of ion velocity in two directions, Planet. Space Sci., 37, 493-502, 1989.

Opgenoorth, H.J., B.J.I. Bromage, D. Fontaine, C. La Hoz, A. Huuskonen, H. Kohl, U.P. Løvhaug, G. Wannberg, G. Gustavsson, J.S. Murphree, G. Marklund, R. Lundin, T.A. Potemra, S. Kirkwood, E. Nielsen and J-E. Wahlund, Coordinated observations with EISCAT and the VIKING satellite: The decay of a westward travelling surge, Ann. Geophys., 7, 479-500, 1989.

Parish, H., T.J. Fuller-Rowell, D. Rees, T.S. Virdi and P.J.S. Williams, Numerical simulations of the seasonal response of the thermosphere to propagating tides, Adv. Space Res., 9, 287-291, 1989.

Pollari, P., A. Huuskonen, E. Turunen and T. Turunen, Range ambiguity effects in a phase coded D-region incoherent scatter radar experiment, J. atmos. terr. Phys., 51, 937-945, 1989.

Quegan, S., The influence of convection on the structure of the high-latitude ionosphere, Phil. Trans. Roy. Soc., A, 328, 119-137, 1989.

Rasinkangas, R., K. Kaila and T. Turunen, Comparison of the lower border of aurora determined by two optical emission ratio models, Planet. Space Sci., 37, 1117-1126, 1989.

Robinson, T.R., The heating of the high latitude ionosphere by high power radio waves, Phys. Rev., 179, 179-209, 1989.

Schlegel, K. and D.R. Moorcroft, EISCAT as a tristatic auroral radar, J. Geophys. Res., 94, 1430-1438, 1989.

Shen Chang-Shou, Luo Yi and K. Schlegel, The feature of the ionosphere in the auroral zone and the magnetosphere-ionosphere coupling, Chinese J. Space Sci., 9, 127-135, 1989.

Shen Chang-Shou, Zi Min-Yun and K. Schlegel, A case study of the ionospheric morphology at high latitude, Acta Geophys. Sinica, 32, 262-269, 1989.

Suvanto, K., Ion cyclotron instability driven by non-thermal F-region plasma, Planet. Space Sci., 37, 1-4, 1989.

Suvanto, K., M. Lockwood and T.J. Fuller-Rowell, The influence of anisotropic F-region ion velocity distributions on ionospheric ion outflows into the magnetosphere, J. Geophys. Res., 94, 1347-1358, 1989.

Suvanto, K., M. Lockwood, K.J. Winser, A.D. Farmer and B.J.I. Bromage, Analysis of incoherent scatter spectra from non-Maxwellian plasma, Adv. Space Res., 9, 103-106, 1989.

Suvanto, K., M. Lockwood, K.J. Winser, A.D. Farmer and B.J.I. Bromage, Analysis of incoherent scatter radar data from non-thermal F-region plasma, J. atmos. terr. Phys., 51, 483-495, 1989.

Taieb, C., Simulation of the plasma density in the polar cap F-region with a convection field obtained from EISCAT observations, Ann. Geophys., 7, 355-363, 1989.

Taylor, M.J., A.P. van Eyken, H. Rishbeth, G. Witt, N. Witt and M.A. Clilverd, Simultaneous observations of noctilucent clouds and polar mesosphere summer echoes, Planet. Space Sci., 37, 1013-1020, 1989.

Uspensky, M.V., A.V. Kustov, P.J.S. Williams, A. Huuskonen, J. Kangas and E. Nielsen, Effect of unresolved electrojet microstructure on measurements of irregularity drift velocity in auroral radar backscatter, Adv. Space Res., 9, 119-122, 1989.

Virdi, T.S. and P.J.S. Williams, Observations of tidal modes in the lower thermosphere using EISCAT, Adv. Space Res., 9, 83-86, 1989.

Wahlund, J-E. and H.J. Opgenoorth, EISCAT observations of strong ion outflows from the F-region ionosphere during auroral activity: Preliminary results, Geophys. Res. Lett., 16, 727-730, 1989.

Wahlund, J-E., H.J. Opgenoorth and P. Rothwell, Observations of thin auroral ionization layers by EISCAT in connection with pulsating aurora, J. Geophys. Res., 94, 223-233, 1989.

Williams, P.J.S., Observations of atmospheric gravity waves with incoherent scatter radar, Adv. Space Res., 9, 65-72, 1989.

Williams, P.J.S. and T.S. Virdi, EISCAT observations of tidal modes in the lower thermosphere, J. atmos. terr. Phys., 51, 569-577, 1989.

Williams, P.J.S., T.S. Virdi and S.W.H. Cowley, Substorm processes in the geomagnetic tail and their effect in the nightside auroral zone ionosphere as observed by EISCAT, Phil. Trans. Roy. Soc., A, 328, 173-193, 1989.

Williams, P.J.S., A.P. van Eyken, C. Hall and J. Röttger, Modulations in the Polar Mesosphere Summer Echoes and associated atmospheric gravity waves observed by EISCAT, Geophys. Res. Lett., 16, 1437-1440, 1989.

Winser, K.J., G.O.L. Jones, P.J.S. Williams and M. Lockwood, Observations of large field-aligned flows of thermal plasma in the auroral ionosphere, Adv. Space Res., 9, 57-63, 1989.

Winser, K.J., M. Lockwood, G.O.L. Jones and K. Suvanto, Observations of non-thermal plasmas at different aspect angles, J. Geophys. Res., 94, 1439-1449, 1989.

Winser, K.J., M. Lockwood, G.O.L. Jones and K. Suvanto, Radar observations of non-thermal plasmas at different aspect angles, Adv. Space Res., 9, 107-112, 1989.

Publications (Theses, Proceedings, Reports, etc), 1989

PhD THESES

Lilensten, J., Resolution de l'equation de transport et application dans le plasma ionospherique, These de doctorat, Polytechnique de Grenoble, 1989.

McCrea, I.W., Radar observations of energy deposition and dissipation in the high-latitude ionosphere, Ph.D. Thesis, University of Leicester, 1989.

Natorf, L., Incoherent scatter observations of acoustic gravity waves in the auroral zone, Ph.D. Thesis, Polish Academy of Sciences, Warsaw, 1989.

Parish, H.F., Modelling the response of the thermosphere to lower atmosphere tides, Ph.D. Thesis, University of London, 1989.

Suvanto, K., Non-Maxwellian ion velocity distributions in the ionospheric F-region, Ph.D. Thesis, University of London, 1989.

Vallinkoski, M., Error analysis of incoherent scatter radar measurements, Ph.D Thesis, University of Helsinki, 1989.

M.Sc. THESES

Ekjeholm, B-T., First gyro line observations with the EISCAT VHF radar, Cand. scient. Thesis, University of Tromsø, 1989.

Mercer, A., Quasi-periodic variations in auroral zone plasma velocities, M.Sc Thesis, University of Wales, 1989.

Moen, J., Conductivity studies in the auroral ionosphere by EISCAT, Cand. scient. Thesis, University of Tromsø, 1989.

PROCEEDINGS and REPORTS

Brekke, A. and C. Hall, Quiet time conductivities of the auroral ionosphere, AGARD Conf. Proc., 441, 24.1-24.17, Neuilly, 1989.

Figueroa, D. and H. Kohl, Calculation of the temperature and velocity of the neutral gas using CP-3 data, AGARD Conf. Proc., 441, 25.1-25.4, Neuilly, 1989.

Franke, S.J, C. La Hoz, J. Röttger and C.H. Liu, Frequency domain interferometry of PMSE, Handbook for MAP, 28, 210-221, Ed. C.H. Liu and B. Edwards, 1989.

Glatthor, N. and R. Hernandez, Temperature anisotropy of drifting ions in the auroral F-region, observed by EISCAT, Max-Planck-Institut für Aeronomie report, MPAE-W-100-89-26, 1989.

Hall, C.M., A. Brekke, U.P. Løvhaug and B.N. Mæhlum, Background electrodynamics measured by EISCAT during the NEED campaign, Proc. 9th ESA/PAC symposium, ESA SP-291, 153-157, 1989.

Jones, G.O.L., K.J. Winser, J. Röttger, C. La Hoz and S.J. Franke, A statistical review of the EISCAT PMSE 1988 data, Handbook for MAP, 28, 126-130, Ed. C.H. Liu and B. Edwards, 1989.

La Hoz, C., J. Röttger, M.T. Rietveld, G. Wannberg and S.J. Franke, The status and planned developments of EISCAT in mesosphere and D-region experiments, Handbook for MAP, 28, 476-488, Ed. C.H. Liu and B. Edwards, 1989.

La Hoz, C., J. Röttger and S.J. Franke, Dynamic spectra of PMSE measured by EISCAT at 224 MHz, Handbook for MAP, 28, 248-256, Ed. C.H. Liu and B. Edwards, 1989.

La Hoz, C., J. Röttger and S.J. Franke, Spatial interferometry measurements with the EISCAT VHF radar, Handbook for MAP, 28, 185-191, Ed. C.H. Liu and B. Edwards, 1989.

Løvhaug, U.P., Ionosfæriske forstyrrelser - kritisk for GPS? Erfaringer fra EISCATs UHF radar, Proceedings of Geodesidagene 1989, Stjørdalen, 16-17 November 1989.

McCrea, I.W., T.R. Robinson M. Lester and T.B. Jones, Ion heating events observed by the EISCAT radar, AGARD Conf. Proc., 441, 26.1-26.10, Neuilly, 1989.

Mauelshagen, H-P. and K. Schlegel, Atmospheric gravity waves in the auroral source region of TIDs studied with the EISCAT CP-2 data, AGARD Conf. Proc., 441, 28.1-28.14, Neuilly, 1989.

Röttger, J., Mean, tidal and fluctuating winds in the middle atmosphere and lower thermosphere observed during MAP/WINE in northern Scandinavia, Handbook for MAP, 27, 179-209, Ed. B. Edwards, 1989.

Röttger, J., The interpretation of MST radar echoes: the present knowledge of the scattering/reflection and the irregularity generation mechanism, Handbook for MAP, 28, 68-82, Ed. C.H. Liu and B. Edwards, 1989.

Röttger, J., U-P Hoppe and C. Hall, EISCAT observations during MAC/SINE and MAC/EPSILON, Handbook for MAP, 27, 370-376, Ed. B. Edwards, 1989.

Röttger, J. and C. La Hoz, Fine structure of Doppler spectra of polar mesosphere summer echoes (PMSE) observed with the EISCAT 224 MHz radar, Handbook for MAP, 28, 107-114, Ed. C.H. Liu and B. Edwards, 1989.

Röttger, J., C. La Hoz, S.J. Franke and C.H. Liu, Gravity wave steepening and tilting detected in high resolution Doppler spectra of polar mesosphere summer echoes (PMSE) observed with the EISCAT 224 MHz radar, Handbook for MAP, 28, 267-277, Ed. C.H. Liu and B. Edwards, 1989.

Röttger, J., M.T. Rietveld, C. La Hoz, T. Hall, M.C. Kelly and W. Swartz, Polar mesosphere summer echoes observed with the EISCAT 933 MHz and CUPRI 46.9 MHz radars, Handbook for MAP, 28, 168-178, Ed. C.H. Liu and B. Edwards, 1989.

Schlegel, K., Auroral backscatter characteristics (at 16 cm wavelength and large aspect angles), Max-Planck-Institut für Aeronomie report, MPAE-W-05-89-24, 1989.

Schlegel, K. and D.R. Moorcroft, Unusual echoes observed with EISCAT, Max-Planck-Institut für Aeronomie report, MPAE-W-05-89-13, 1989.

Wannberg, G., J. Röttger, C. La Hoz and P.J.S. Williams, Long range planning for development of full MST capabilities at EISCAT, Handbook for MAP, 28, 544-548, Ed. C.H. Liu and B. Edwards, 1989.

Wannberg, G., J. Röttger and T. Sturk, Gain and phase calibration of the EISCAT receivers in MST applications, Handbook for MAP, 28, 549-555, Ed. C.H. Liu and B. Edwards, 1989.

Williams, P.J.S., A.P. van Eyken, C. Hall and J. Röttger, Polar mesosphere summer echoes and associated atmospheric gravity waves, Proc. 9th ESA/PAC symposium, ESA SP-291, 187-191, 1989.

SUPPLEMENT 1987

Blanc, M., D. Fontaine, R. Glowinski and L. Reinhart, Numerical simulation of the magnetospheric electron transport phenomena by finite elements and a method of characteristics, Series: 'Applied Mathematics', Gordon and Breach, Science Publishers, Inc., USA, 1987.

VIDEO

Nuit d'Aurores: les relations soleil-terre,
D. Alcaydé, M. Blanc, D. Fontaine,
B. Pedersen Producer: D. Pedersen.
French version: 1988
English version: 1989

EISCAT REPORTS AND MEETINGS

Reports 1989:

EISCAT Technical Note, 1989/49, Error Analysis of Incoherent Scatter Radar Measurements, Vallinkoski, M., PhD Thesis, University of Helsinki, 1989.

EISCAT Technical Note, 1989/50, Proceedings of the EISCAT Summer School, Tromsø, Norway, August 1986, C. La Hoz and A. Brekke (Editors).

EISCAT Technical Note, 1989/51, Non-Maxwellian Ion Velocity Distribution in the Ionospheric F-region, Suvanto, K., PhD Thesis, University of London, 1989.

PMSE87/88, The Observations of Polar Mesosphere Summer Echoes with EISCAT in Summer 1987 and 1988; Compilation of Reports and Publications, J. Röttger (Editor), 1989.

Report presented to the EISCAT Council, 'An HF Heating Facility for EISCAT: The Scientific Case', EISCAT-Heating Working Group, Robinson, T.R. (Chairman), E. Mjølhus, M.T. Rietveld, P. Stubbe and B. Thide, October 1989.

EISCAT Information Leaflet, A.P. van Eyken and J. Röttger (Editors).

EISCAT Annual Report 1988.

Meeting reports:

EISCAT Meetings No. 89/14, Proceedings of the EISCAT Annual Review Meeting 1989, Hetta, Finland, 27 February - 2 March 1989, G. Wannberg (Editor).

Meetings 1989:

COUNCIL	33rd meeting, 9-10 November	Didcot, UK
SAC	36th meeting, 4 June	Sigtuna, Sweden
	37th meeting, 17-18 October	Kiruna, Sweden
AFC	32nd meeting, 7 April	Hamburg, Federal Republic of Germany
	33rd meeting, 28 September	Tromsø, Norway

BALANCE SHEET AT 31 DECEMBER 1989

MSEK

Assets	At 31 Dec 1988	Additions			Depre-ciations	At 31 Dec 1989
		Pool	Cap Op	Other		
FIXED ASSETS						
Buildings	8.0				0.2	7.8
Transmitters	29.1	0.1			1.8	27.4
UHF Antennas	13.4				1.3	12.1
VHF Antenna	17.1				1.5	15.6
Computers, etc	4.7		0.6		1.1	4.2
Other	2.4		1.0		0.9	2.5
Total	74.7	0.1	1.6		6.8	69.6
CURRENT ASSETS						
Debtor	1.0					1.0
Prepayments and accrued income	0.3					0.3
Cash and Ordinary Bank Accounts	5.9					7.4
Special Account	0.2					2.3
Total	7.4					11.3
GRAND TOTAL	82.1					80.9

MSEK

Liabilities	At 31 Dec 1988	At 31 Dec 1989
CAPITAL		
Contributions		
Pool	92.7	92.8
Capital Operating	15.6	17.2
In Kind	25.1	25.1
Other	0.4	0.4
	133.8	135.5
Depreciations	59.1	65.9
Total Capital	74.7	69.6
RESERVES		
Pool	0.6	0.5
Capital Operating	0.9	1.0
Other	2.6	4.0
Total Reserves	4.1	5.5
Special Account	0.2	2.3
LIABILITIES		
Provisions	0.2	0.4
Other Liabilities	2.9	3.1
Total Liabilities	3.1	3.5
GRAND TOTAL	82.1	80.9

Total budget in 1989 (MSEK):

		MSEK
Recurrent chapter:	Personnel:	8.56
	Administration:	3.94
	Operations:	4.21
	Total:	16.72
Capital Investment chapter:		2.60

Totals may not match because of rounding. MSEK = Million Swedish Crowns

EISCAT SCIENTIFIC ASSOCIATION 1989

31 December 1989

	France	Finland	Federal Republic of Germany	Norway	Sweden	United Kingdom
COUNCIL	P. Bauer A. Berroir G. Caudal	J. Kangas A. Siivola	W.I. Axford G. Haerendel G. Preiss	O. Havnes B. Benterud	B. Hultqvist M.O. Ottosson	W.J.G. Beynon T.B. Jones* B.R. Martin
SAC	D. Fontaine W. Kofman	T. Turunen*	W. Baumjohann K. Rinnert	N. Bjørnå	H. Opgenoorth	S.W.H. Cowley P.J.S. Williams
AFC	C. Blamont	O. Ranta	M. Meinecke*	A. Andersen	J. Gustavsson	D. Morrell

SAC = Scientific Advisory Committee AFC = Administrative and Finance Committee * = Chairman

EISCAT Senior Staff

Director: J. Röttger (on secondment from MPG)
Deputy Director: G. Wannberg
Business Manager: P. Hagström

Senior Scientist: A.P. van Eyken
Head of Computer Operations: S. Buchert

Site Leaders: Kiruna: I. Wolf
Sodankylä: M. Postila
Tromsø: R. Jacobsen

THE EISCAT ASSOCIATES

CNRS
Centre National de la Recherche Scientifique
France

SA
Suomen Akatemia
Finland

MPG
Max-Planck-Gesellschaft
Federal Republic of Germany

NAVF
Norges Almenvitenskapelige Forskningsråd
Norway

NFR
Naturvetenskapliga Forskningsrådet
Sweden

SERC
Science and Engineering Research Council
United Kingdom